ACS APPLIED MATERIALS & INTERFACES

www.acsami.org

Research Article

Injectable Bacteria-Sensitive Hydrogel Promotes Repair of Infected Fractures via Sustained Release of miRNA Antagonist

Chenyan Yu,[#] Lang Chen,[#] Wu Zhou,[#] Liangcong Hu, Xudong Xie, Ze Lin, Adriana C. Panayi, Xingjie Zhan, Ranyang Tao, Bobin Mi,[*] and Guohui Liu[*]

Cite This: *ACS Appl. Mater. Interfaces* 2022, 14, 34427−34442

Read Online

ACCESS | Metrics & More | Article Recommendations | Supporting Information

ABSTRACT: Fracture nonunion can result in considerable physical harm and limitation of quality of life in patients, exerting an extensive economic burden to the society. Nonunion largely results from unresolved inflammation and impaired osteogenesis. Despite advancements in surgical techniques, the indispensable treatment for nonunion is robust anti-inflammation therapy and the promotion of osteogenic differentiation. Herein, we report that plasma exosomes derived from infected fracture nonunion patients (Non-Exos) delayed fracture repair in mice by inhibiting the osteogenic differentiation of bone marrow stromal cells in vivo and in vitro. Unique molecular identifier microRNA-sequencing (UID miRNA-seq) suggested that microRNA-708-5p (miR-708-5p) was overexpressed in Non-Exos. Mechanistically, miR-708-5p targeted structure-specific recognition protein 1, thereby suppressing the Wnt/β-catenin signaling pathway, which, in turn, impaired osteogenic differentiation. AntagomicroRNA-708-5p (antagomiR-708-5p) could partly reverse the above process. A bacteria-sensitive natural polymer hyaluronic-acid-based hydrogel (HA hydrogel) loaded with antagomiR-708-5p exhibited promising effects in an in vivo study through antibacterial and pro-osteogenic differentiation functions in infected fractures. Overall, the effectiveness and reliability of an injectable bacteria-sensitive hydrogel with sustained release of agents represent a promising approach for infected fractures.

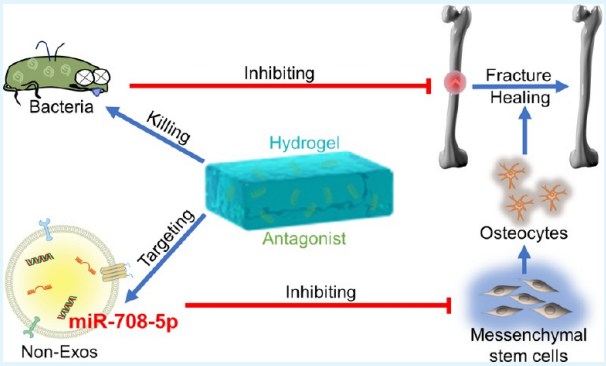

KEYWORDS: *exosomes, hydrogel, infected fracture nonunion, BMSCs, miR-708-5p*

1. INTRODUCTION

Fracture nonunion, that is, the failure of a fracture to heal after proper therapy, has been reported to occur in as high as 5−10% of patients with fractures, resulting in severe pain, physical disability, and extensive healthcare costs.[1] The causes of fracture nonunion can be broadly classified into four clusters: mechanical, infectious, vascular, and surgical.[2] Studies have reported that the rate of incidence of fracture-related infection (FRI) varies from 15 to 55% after an open fracture.[3−5] Current treatments focus on the following aims: debridement, antibacterial treatment, promotion of fracture repair, soft-tissue coverage, prevention of chronic osteomyelitis, and restoration of limb function.[6]

Although polymethylmethacrylate (PMMA) and calcium sulfate (CS) are common local antibiotic carriers, PMMA has low biodegradability, while CS may result in complications due to aseptic wound drainage.[7,8] Besides, topical antibiotics increase the risk of antibiotic resistance. Autologous bone grafts present a series of advantages in fracture repair, but only few cells in grafts have the ability to differentiate into osteoblasts. In addition, donor bone extraction causes inevitable morbidity.[9]

Bone marrow stromal cells (BMSCs), characterized by excellent osteogenic differentiation potential, play an important role in the process of fracture healing and can be used as an alternative treatment for fracture nonunion.[10−12] Previous studies have explored multiple regulatory mechanisms involved in the osteogenic differentiation of BMSCs, but the mechanism through which BMSC osteogenic differentiation is involved in the delayed healing of fractures remains unclear and requires further investigation.

Exosomes are nano-sized extracellular vesicles, ranging from 30 to 200 nm in diameter, which are almost universally secreted by all cells.[13,14] Formed in the endosomal network, exosomes are secreted into the blood and act as vehicles transporting proteins, nucleic acids, and metabolites encapsulated in them to their recipient cells, altering the biological activity of their receptors.[15] Previous studies have reported the

Received: May 13, 2022
Accepted: July 13, 2022
Published: July 22, 2022

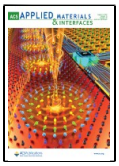

https://doi.org/10.1021/acsami.2c08491
ACS Appl. Mater. Interfaces 2022, 14, 34427−34442

use of exosomes in the treatment of inflammatory diseases with some mediated by miRNA, a class of non-coding RNA molecules capable of regulating gene expression by binding to complementary regions in the target mRNAs.[16−21] Furthermore, El-Jawhari et al. provided evidence that the serum from fracture nonunion patients might hinder the osteogenic differentiation of BMSCs.[22] Therefore, we hypothesize that plasma-derived exosomes may be involved in the delayed healing of infected nonunion repair.

We, therefore, collected Non-Exos and NC-Exos and applied these both in vitro and in vivo to investigate their effects on the osteogenesis of BMSCs in a nonunion model (Scheme 1a). To explore the potential underlying mechanisms, we performed a UID miRNA sequence to identify any differentially expressed miRNAs and carried out a series of experiments to verify that exosomal miR-708-5p inhibits the osteogenesis of BMSCs by targeting structure-specific recognition protein 1 (SSRP1) and suppressing Wnt signaling (Scheme 1b). Additionally, a previous study by our group presented evidence of the antibacterial, self-healing, and tissue-adhesive properties of a novel injectable HA hydrogel.[23] In addition, the hydrogel could preserve the biological properties of the active substance.[23] Here, we use the antimicrobial hydrogel preloaded with antagomiR-708-5p for the treatment of murine femoral fractures with internal fixation with or without *Staphylococcus aureus* infection. Compared with a control group, the HA hydrogel loaded with the miR-708-5p inhibitor effectively promoted the infected fracture repair (Scheme 1c). We also attempted to explore the source of exosomes by co-culturing macrophages and *S. aureus* and found that macrophage-derived exosomes with miR-708-5p enrichment inhibited the osteogenic differentiation of BMSCs. Taken together, the results showed that hydrogel loaded with antagomiR-708-5p has significant pro-osteogenesis and antibacterial properties, promoting infected fracture healing.

Scheme 1. (a) Isolation of Exosomes from Plasma; (b) Osteoblast Differentiation of BMSCs Inhibited by Exosomal miR-708-5p Derived from Male Patients Diagnosed with Fracture Nonunion; and (c) Antibacterial Hydrogel@ antagomiR-708-5p for the Therapy of Infected Nonunion Fractures

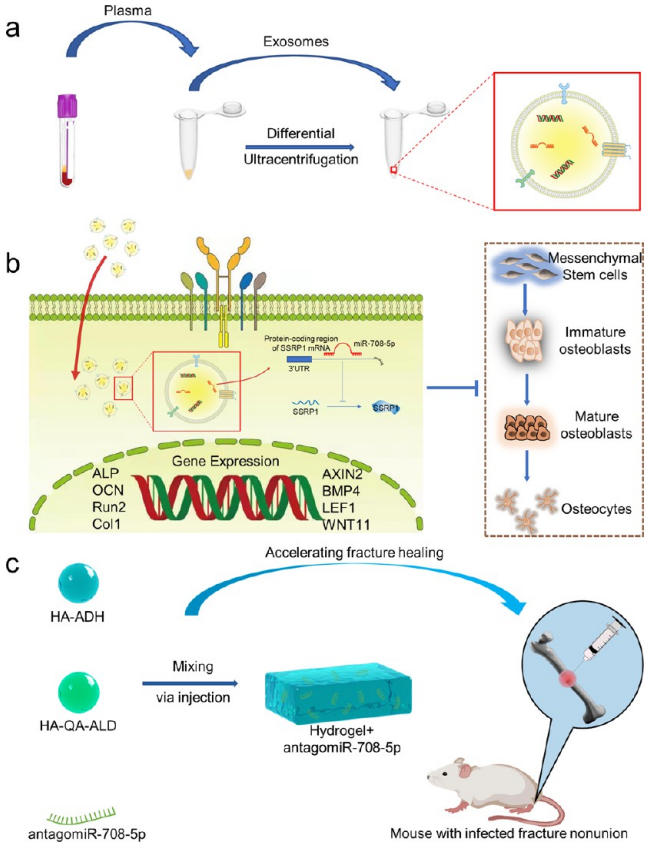

2. RESULTS

2.1. Characteristics of Exosomes from Volunteers with or without Fracture Nonunion. We used an ultracentrifugation assay to isolate exosomes from volunteers' plasma. To verify the exosome isolation, we observed typical "cup-shaped" exosomal vesicles by using transmission electron microscopy (TEM) and measured exosome particle size and concentration by using NanoFCM N30E (Figure 1a,b). The results showed that in exosomes from the control group, vesicles with a particle size of 30−150 nm accounted for 98.2% of the total number of particles and the concentration was 4.67 × 10^8/mL, while for exosomes from the nonunion group, vesicles with a particle size of 30−150 nm accounted for 90.35% of the total number of particles and the concentration was 3.55 × 10^8/mL (Figure 1c). Western blot showed that TSG101 was weakly positive, CD81 was positive, and calnexin was negative (Figure 1d). These characteristics are consistent with previous reports for exosome identification.[24,25] These results confirmed that we extracted purified exosomes from plasma.

2.2. Non-Exos Impeded Fracture Healing in Mice. To find out whether Non-Exos affect fracture healing in mice, we constructed a mouse model with internal fixation of right middle femur fractures. Phosphate-buffered saline (PBS), 50 μg/mL NC-Exos, 50 μg/mL Non-Exos, and 100 μg/mL Non-Exos were locally administered into the fracture site every 3 days. DIR-labeled exosomes were shown on small animal live imaging (Figure 2a). Mice (n = 3) were sacrificed 21 days after surgery, and the total protein was extracted from bone callus for detecting changes in the expression of osteogenesis-related proteins. The results revealed that Non-Exos inhibited the expression of the osteogenesis-related proteins Col1, Runx2, ALP, and OCN (Figure 2b). To dynamically observe the effect of Non-Exos on fracture healing, we used small animal biopsies to visualize the fracture sites on days 7, 14, and 21 after surgery and showed that Non-Exos delayed the formation of bone callus and the formation of bony bridging at the fracture site (Figure 2c). MicroCT 3D reconstruction results on postoperative day 14 showed lower bone callus formation and larger fracture gaps in the 50 and 100 μg/mL Non-Exos-treated groups than in the control group. On postoperative day 21, a larger fracture gap with a less-bony callus tissue was seen in the Non-Exos-treated group. The bone volume/total volume (BV/TV) and the trabecular thickness (Tb.Th) at the fracture junction were significantly decreased in the 50 μg/mL Non-Exos- and 100 μg/mL Non-Exos-treated groups compared to the NC-Exos-treated group (P < 0.05; Figure 2d−f). HE/Alcian blue staining showed a decreased bone area and increased cartilage area in the 50 and 100 μg/mL NC-Exos-treated groups compared to the PBS or NC-Exos-treated group (Figure 2g−i). All results revealed that Non-Exos have an

https://doi.org/10.1021/acsami.2c08491
ACS Appl. Mater. Interfaces 2022, 14, 34427−34442

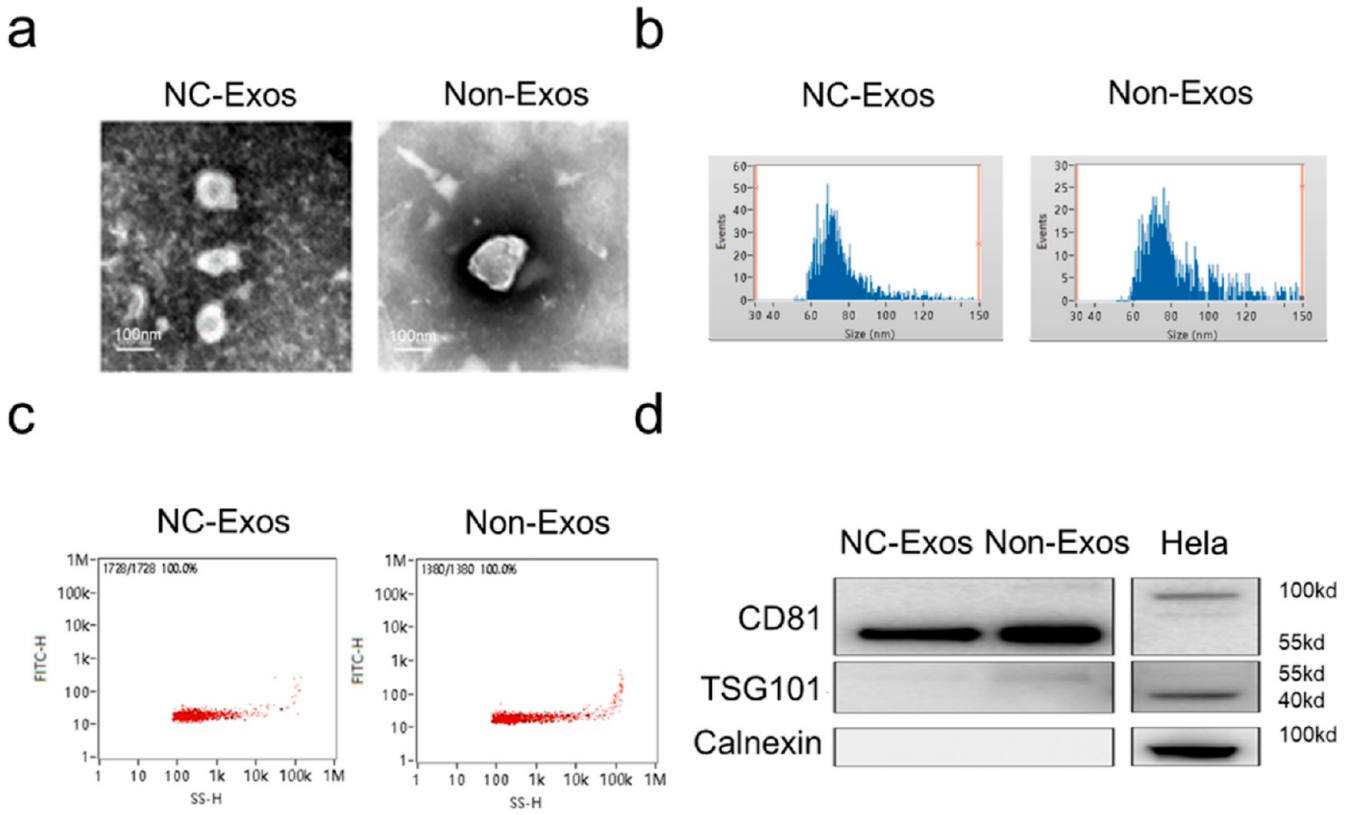

Figure 1. Characteristics of exosomes from patients with or without infected fracture nonunion (n = 3 per group). (a) NC-Exos and Non-Exos imaging with TEM. (b,c) Particle size distribution and concentration of NC-Exos and Non-Exos measured with NanoFCM (Flow Bio Flow NanoAnalyzer). (d) Positive protein marker CD81, TSG101, and negative protein marker calnexin in the two kinds of exosomes.

inhibitory effect on fracture healing and osteogenesis in murine fracture models.

2.3. Non-Exos Inhibited the Osteogenic Differentiation of BMSCs. To investigate how the Non-Exos influenced fracture healing, we treated BMSCs with 25 μg/mL NC-Exos, 25 μg/mL Non-Exos, or 50 μg/mL Non-Exos. To verify that exosomes can be taken up by BMSCs, exosomes were stained with PKH26, and the cytoskeleton was stained with phalloidin. Fluorescence imaging with confocal microscopy showed red glowing exosomes in BMSCs and verified that NC-Exos and Non-Exos could be taken up by BMSCs (Figure 3a). BMSCs were then harvested in passage 4 and treated with PBS, 25 μg/mL NC-EXOS, 25 μg/mL Non-Exos, and 50 μg/mL Non-Exos. After treatment for 24 h, quantitative polymerase chain reaction (qPCR), western blot, ALP staining, and Alizarin red staining (ARS) were performed to explore the effect of Non-Exos on the osteogenic differentiation of BMSCs. qPCR and western blotting indicated that the osteogenesis-related protein expression was significantly decreased in the Non-Exos-treated groups (Figure 3b,c). ALP staining and ARS indicated that the ALP activity and calcium nodule formation were partially prohibited in the Non-Exos-treated groups (Figure 3d−g). All these results displayed the Non-Exos impediment of BMSCs osteogenic differentiation.

2.4. Non-Exos Contained High Levels of miR-708-5p and Transferred miR-708-5p to BMSCs. We collected three samples of Non-Exos and three samples of NC-Exos for UID microRNA-seq (Table 1). Compared to NC-Exos, Non-Exos contained more miR-708-5p, miR-590-5p, and other novel miRNAs (Figure 4a). By treating BMSCs with agomiR-590-5p, agomiR-708-5p, and agomiR-negative control and inducing the osteogenic differentiation of BMSCs for ALP staining, we found that agomiR-590-5p had no visible effects on the ALP activity of BMSCs, while agomiR-708-5p showed marked suppression (Figures 4b, 5d). qPCR verified that miR-708-5p increased in Non-Exos compared to that in NC-Exos (Figure 4c). We further assessed whether the miRNAs encapsulated in exosomes could perform their functions when the exosomes were taken up by BMSCs. Treatment with PBS, 25 μg/mL NC-Exos, 25 μg/mL Non-Exos, or 50 μg/mL Non-Exos showed that although treatment of BMSCs with both sources of exosomes increased intracellular miR-708-5p, the Non-Exos-treated group showed a higher level of miR-708-5p than the NC-Exos-treated group as analyzed by qPCR (Figure 4d). The result led us to consider whether the differential expression of miR-708-5p played a significant part in the inhibition of osteogenic differentiation of BMSCs by Non-Exos. Therefore, BMSCs were treated with PBS, NC-Exos, and NC-Exos + antagomiR-708-5p (100 nM). qPCR and western blotting were conducted to investigate the effect of the three treatments on the expression of osteogenic-related proteins. The results demonstrated that antagomiR-708-5p can reverse the inhibition of osteogenesis-related protein expression caused by Non-Exos at the RNA and protein levels (Figure 4e,f). ALP staining and ARS pointed that antagomiR-708-5p was restored partly and even reversed the decreased ALP activity and mineralization of BMSC osteogenic differentiation resulting from Non-Exos treatment (Figure 4g−j). All outcomes indicated that Non-Exos suppressed the osteogenic differentiation of BMSCs mediated in part by miR-708-5p contained in the Non-Exos group.

https://doi.org/10.1021/acsami.2c08491
ACS Appl. Mater. Interfaces 2022, 14, 34427−34442

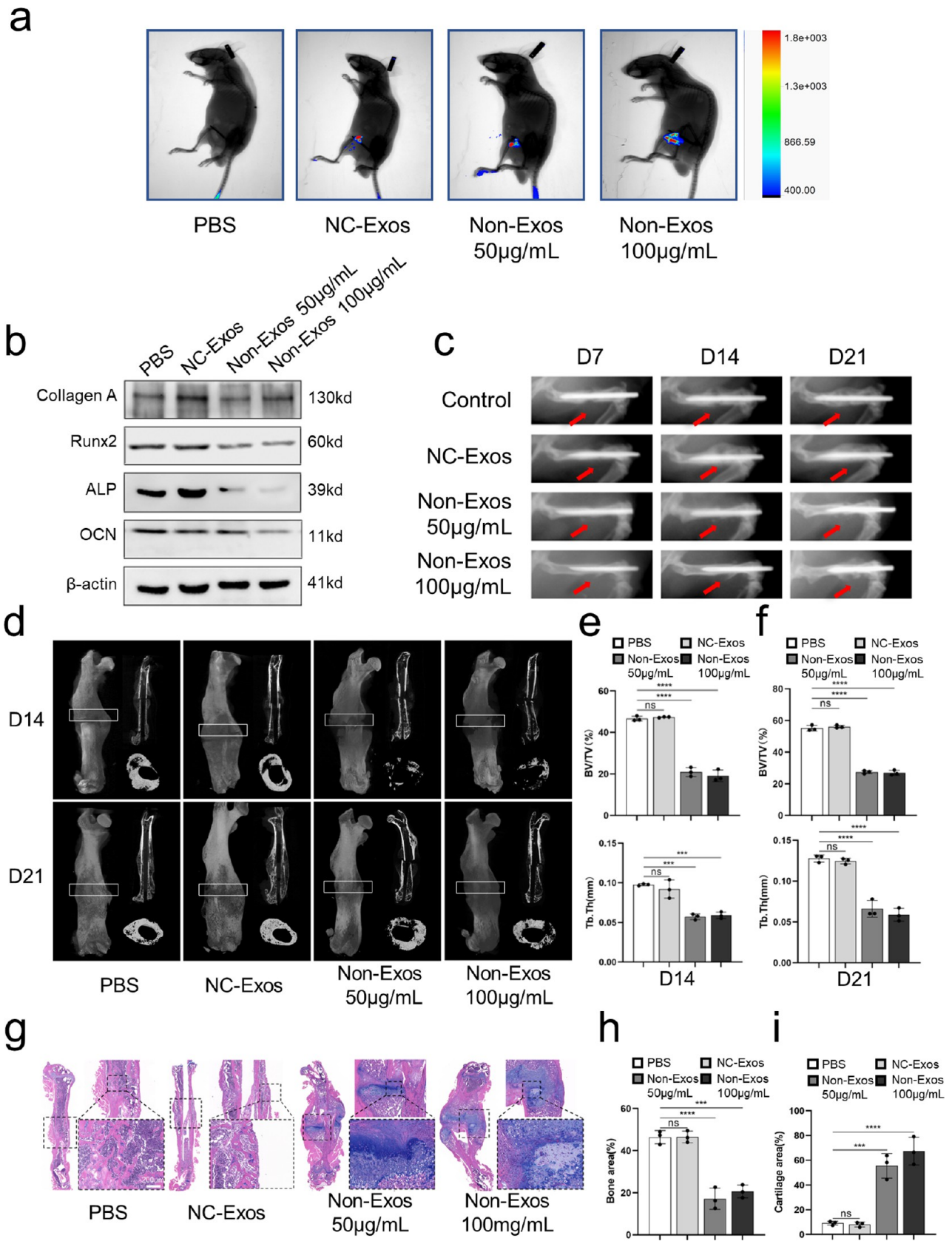

Figure 2. Non-Exos delay fracture healing in vivo. A middle femur fracture with stable internal fixation was induced in 40 mice, which were randomly divided into four groups (n = 10 per group), treated with 20 μL of PBS, 50 μg/mL NC-Exos, 50 μg/mL Non-Exos, or 100 μg/mL Non-Exos locally injected to the fracture site once daily for 3 days until sacrifice. (a) In vivo fluorescence imaging with the FX PRO imaging system (BRUKER, Karlsruhe, Germany) outlined the location of DIR-labeled exosomes. (b) Western blot analysis of the protein expression levels of Col1, Runx2, ALP, and osteocalcin in bone callus from the femurs of mice. (c) Representative images of fracture sites taken with the in vivo FX PRO imaging system (BRUKER, Karlsruhe, Germany) on days 7, 14, and 21 post-surgery. (d) MicroCT images of femurs harvested from mice on days

https://doi.org/10.1021/acsami.2c08491
ACS Appl. Mater. Interfaces 2022, 14, 34427−34442

Figure 2. continued

14 and 21 post-surgery. White box indicating the regions of interest (ROI) in the analysis of microCT. (e,f) Assessment of microCT parameters (BV/TV, Tb.Th) of the bone callus from the four different groups of mice (n = 3). (g) HE and Alcian blue staining of femurs harvested from mice on day 21 post-surgery. (h,i) Area of bone and cartilage of the bone callus from mice on day 21 post-surgery calculated with ImageJ. Data are presented as means ± SD from three independent experiments. *p < 0.05, **p < 0.01, ***p < 0.001, and ****p < 0.0001.

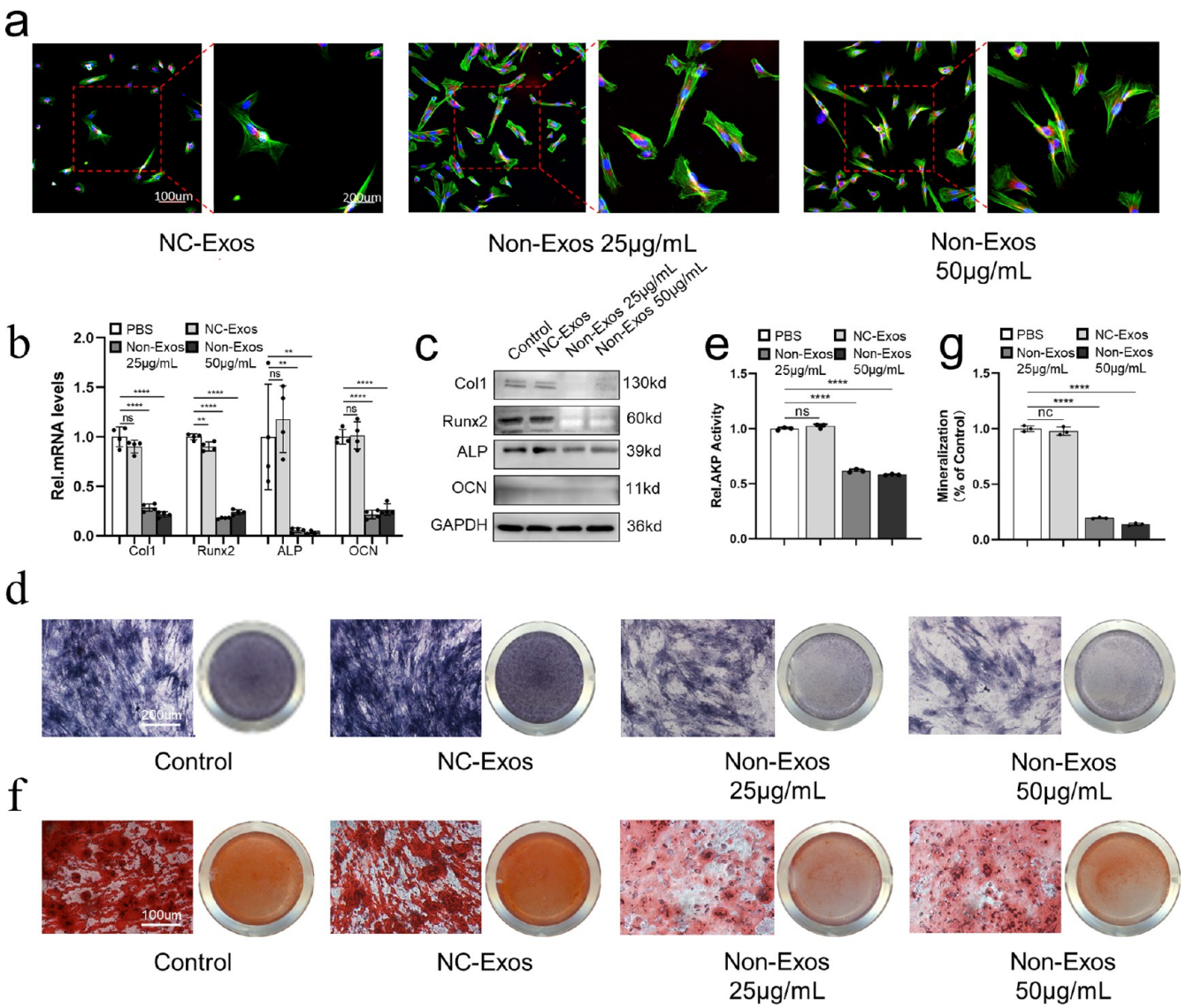

Figure 3. Non-Exos inhibit the osteoblast differentiation of human BMSCs. (a) Confocal microscopy of PKH26-labeled NC-Exos and Non-Exos in human BMSCs with the cytoskeleton stained with phalloidin and the nucleus stained with DAPI. (b) PCR analysis of the mRNA expression levels of Col1, Runx2, ALP, and osteocalcin in human BMSCs treated with PBS, 25 μg/mL NC-Exos, 25 μg/mL Non-Exos, or 50 μg/mL Non-Exos. (c) Western blot analysis of the protein expression levels of Col1, Runx2, ALP, and osteocalcin in human BMSCs treated with PBS, 25 μg/mL NC-Exos, 25 μg/mL Non-Exos, or 50 μg/mL Non-Exos. (d,e) ALP staining of human BMSCs treated with PBS, 25 μg/mL NC-Exos, 25 μg/mL Non-Exos, or 50 μg/mL Non-Exos and analysis of ALP activity with ImageJ. (f,g) ARS staining of human BMSCs treated with PBS, 25 μg/mL NC-Exos, 25 μg/mL Non-Exos, or 50 μg/mL Non-Exos and calculation of the area of mineralization with ImageJ. Statistical data are presented as means ± SD from three independent experiments. *p < 0.05, **p < 0.01, ***p < 0.001, and ****p < 0.0001.

2.5. MiR-708-5p Inhibits Osteogenic Differentiation of the BMSCs. Next, we investigated the impact of miR-708-5p on BMSC osteogenic differentiation. With the administration of PBS, agomiRNA-negative control (agomiR-nc), or agomiR-708-5p, qPCR results showed that the miR-708-5p level was significantly higher in the agomiR-708-5p-treated group (Figure 5a). In addition, we treated BMSCs with antagomiR-708-5p to inhibit endogenous cellular miR-708-5p. ALP staining and ARS demonstrated that agomiR-708-5p markedly suppressed the ALP activity and the mineralization of BMSC osteogenesis differentiation (Figure 5d−g). Conversely, endogenous cellular miR-708-5p inhibition enhanced the ALP activity and increased mineralization in the process of BMSC osteogenesis differentiation (Figure 5d−g). qPCR and western blotting similarly displayed that agomiR-708-5p inhibited the expression of the osteogenesis-related proteins Col1, Runx2,

https://doi.org/10.1021/acsami.2c08491
ACS Appl. Mater. Interfaces 2022, 14, 34427−34442

Table 1. Patient Details of the Fracture Nonunion Patients and the Normal Controls

	patient number	sex	age	wound site
fracture nonunion	1	male	55	left tibia
	2	male	56	right tibia
	3	male	53	right ulnar
normal control	1	male	30	right femur
	2	male	30	right humerus
	3	male	23	right humerus

ALP, and OCN in BMSCs, and inhibition of endogenous miR-708-5p could partially promote the expression of related proteins in the BMSCs (Figure 5b,c). All these results confirmed that miR-708-5p inhibited osteogenic differentiation of BMSCs in vitro. Based on these results, we carried out in vitro experiments to explore from where the exosomes with high level of miR-708-5p expression were derived. F4/80 and CD11b are phenotypic markers of bone marrow-derived macrophages (BMDMs). We identified BMDMs with flow cytometry (Figure S1a). Then, BMDMs were incubated with or without *S. aureus* at a 1:10 multiplicity (cells/bacteria). Exosomes were isolated from the supernatants of a macrophage culture medium by an ultracentrifugation assay. qPCR revealed that, compared with exosomes from macrophages (MD-Exos), exosomes from *S. aureus*-challenged macrophages (MD-bExos) expressed a high level of miR-708-5p (Figure S1b). BMSCs were cultured with the human bone marrow MSC osteogenic differentiation induction medium (Cyagen, HUXMA-90021, Guangzhou, China) and treated with MD-Exos, MD-bExos, and MD-bExos + antagomiR-708-5p, respectively. Western blotting indicated that MD-bExos inhibited the expression of osteogenesis-related protein Col1, Runx2, ALP, and OCN in the process of BMSC osteogenic differentiation, whereas antagomiR-708-5p partly erased the negative effects (Figure S1c). ALP staining and ARS assay further verified the impaired effects of MD-bExos on the osteogenesis and mineralization potential of BMSCs (Figure S1d−g). These in vitro experiments explored the origin of plasma exosomes enriched with miR-708-5p in patients with infected fracture nonunion.

2.6. MiR-708-5p Suppressed Osteogenesis Differentiation and Wnt/β-Catenin Signaling by Targeting SSRP1. To elucidate how miR-708-5p affects the osteogenic differentiation of BMSCs, we used TargetscanHuman_7.1, miRDB, and TarBase_v8.0 to identify the possible target genes of miR-708-5p. As shown in Figure 6a, 10 genes occurred simultaneously in the predicted results of the three databases. After carefully reviewing these studies, we hypothesized that SSRP1 may be a key target gene mediating the suppressive effect of miR-708-5p on osteogenic differentiation.[26] We used a dual-luciferase reporter gene assay to validate miR-708-5p specifically binding to the 3′UTR region of SSRP1. The results showed that when the target region was mutated, agomiR-708-5p could not bind to the complementary region of the target gene to suppress the luciferase activity (Figure 6b). Then, we treated BMSCs with PBS, agomiR-nc, or agomiR-708-5p, and SSRP1 expression was significantly reduced in BMSCs with agomiR-708-5p treatment (Figure 6f,g). The previous study had approved that SSRP1 and Wnt/β-catenin signaling played an important part in the BMSC osteogenic differentiation.[26] We treated the BMSCs with PBS, siRNA-NC, siSSRP1-1 (sense (5′ to 3′) GCCCAGAATGTGTTGTCAA), or siSSRP1-2 (sense(5′ to 3′) GCATTACCTGTTCCTACAA). To verify the efficiency of siSSRP1-1 and siSSRP1-2 knockdown, western blotting was performed. The results revealed the significant knockdown effects of siSSRP1-1, but the knockdown efficiency of siSSRP1-2 was not shown (Figure 6c). Therefore, we elected siSSRP1-1 for subsequent experiments. To verify that the BMSC osteogenic differentiation and Wnt signaling pathway were SSRP1 dependent, we transfected BMSCs with siSSRP1 for qPCR and western blot analyses, ALP staining, and ARS. Western blot results showed that with SSRP1 knocked down, the osteogenic associated protein Col1, Runx2, ALP, and OCN expression decreased (Figure 6d). qPCR showed that with siSSRP1 treatment, the Wnt signaling pathway gene BMP4, AXIN2, Wnt11, and LEF1 mRNA expression were downregulated in contrast to the control group (Figure 6e), which was consistent with previous evidence.[26] β-Catenin protein expression, ALP activity, and the ability of mineralization were significantly suppressed for SSRP1 knocked down BMSCs. However, inhibition could be partly reversed by antagomiR-708-5p (Figure 6h−l). Overall, miR-708-5p specifically targeted SSRP1 and differentially affected osteogenic differentiation and Wnt/β-catenin signaling pathway activity in BMSCs by inhibiting the SSRP1 expression.

2.7. AntagomiR-708-5p Combined with Antibacterial Hydrogel Accelerates Fracture Healing in *S. aureus* Infected Fractures. Our team previously synthesized a multifunctional hyaluronic acid (HA) hydrogel, which was shown to be easily injectable, antibacterial, self-healing, and tissue adhesive.[23] As *S. aureus* is the most common bacteria among FRIs,[27] we applied our antimicrobial, injectable hydrogel preloaded with antagomiR-708-5p (hydrogel@antagomiR-708-5p) to fractures infected with *S. aureus*. The adipic dihydrazide-modified HA (HA-ADH) and quaternary ammonium (QA) and aldehyde HA (HA-QA-ALD) morphology and the process of hydrogel formation are shown in Figure 7a. The swelling and rheological properties and the microstructure of the hydrogel have been previously described.[23] The distribution of antagomiR-708-5p in antagomiR-708-5p-loaded HA hydrogel was visualized with confocal microscopy (Figure 7b). To verify the antibacterial properties of the hydrogel, we incubated *S. aureus* in 48-well plates and treated this with PBS, 2% hydrogel, 3% hydrogel, 4% hydrogel, and 2 μg/mL penicillin. The bacterial solution was applied to agar plates and photographed to observe the colony growth after 16 h. The antimicrobial properties of hydrogels were shown to be dose dependent with 4% hydrogel demonstrating good antibacterial properties (Figure 7c,d). In addition, we did live and dead cell staining to detect the survival of *S. aureus* on the surface of different concentrations of hydrogels separately and did crystalline violet staining to test the effect of hydrogel on biofilm destruction. Our HA hydrogel demonstrated excellent bactericidal effect and little bacterial adhesion and could destroy the bacterial biofilm (Figure S2a,b). To examine the biocompatibility of the hydrogel, we used Cell Counting Kit-8 assay and live and dead cell staining to detect cell death and proliferation. The results show that our hydrogel has good biocompatibility (Figure S3a−c). Our experiments showed that antagomiR-708-5p could be continuously released from the hydrogel (Figure S4). We further examined the impact of hydrogel@antagomiR-708-5p on fracture healing using a mouse fracture model with or without *S. aureus* infection. For a sterile fracture model, bone callus harvested from 21 day postoperative mice was collected for western blotting,

https://doi.org/10.1021/acsami.2c08491
ACS Appl. Mater. Interfaces 2022, 14, 34427−34442

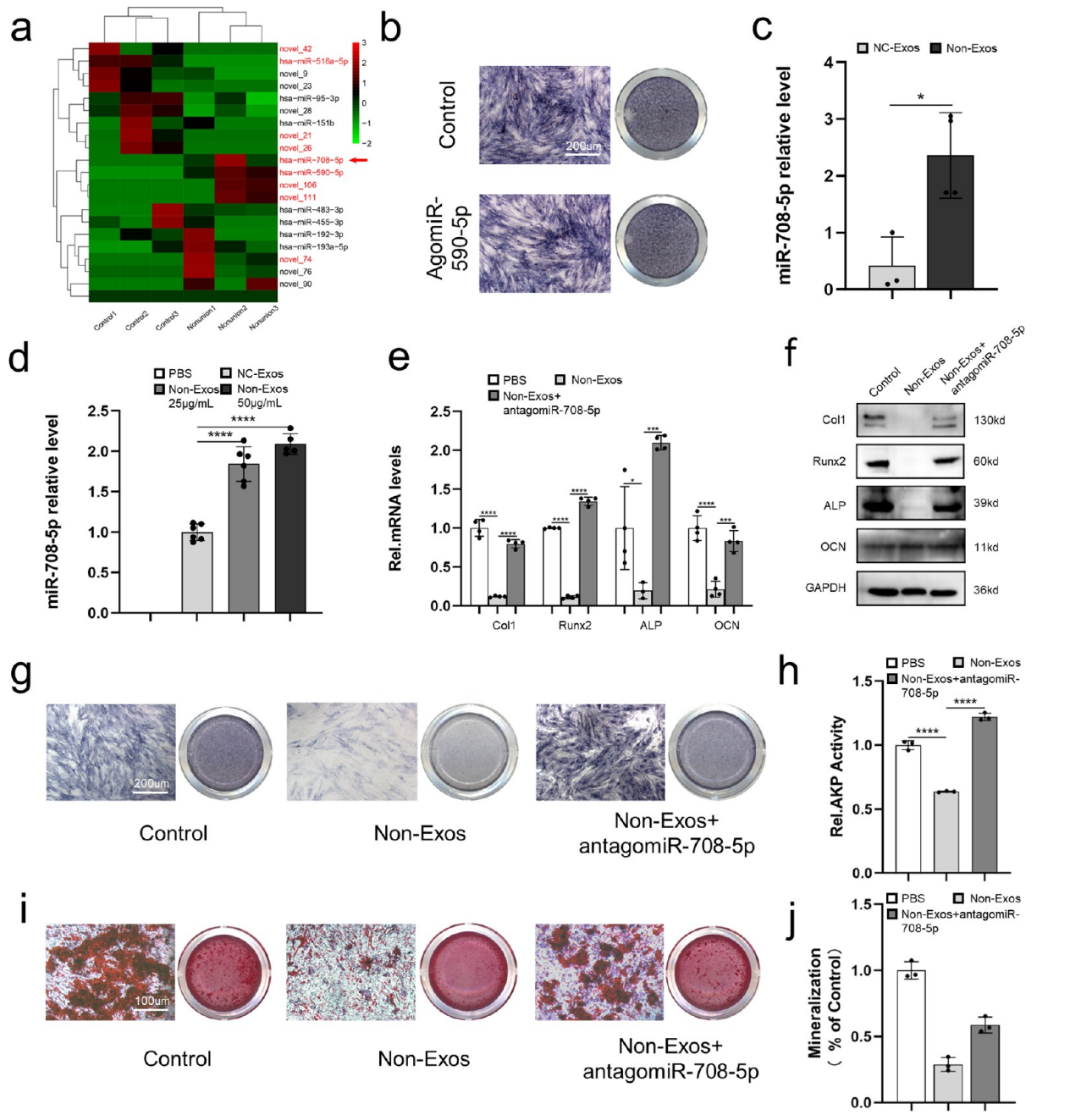

Figure 4. Non-Exos were enriched with miR-708-5p that modulates the osteoblast differentiation of BMSCs. (a) Heat map of miRNAs differently expressed between NC-Exos and Non-Exos. (b) ALP staining of BMSCs treated with agomicroRNA-negative control or agomiR-708-5p after induction of osteogenic differentiation. (c) PCR analysis of miR-708-5p expression in NC-Exos and Non-Exos. (d) PCR analysis of miR-708-5p level in BMSCs treated with PBS, 25 μg/mL NC-Exos, 25 μg/mL Non-Exos, or 50 μg/mL Non-Exos. (e,f) PCR and Western blot analysis of the expression levels of Col1, Runx2, ALP, and osteocalcin in human BMSCs treated with PBS, NC-Exos, or Non-Exos + antagomir-708-5p. (g,h) ALP staining of human BMSCs treated with PBS, Non-Exos, or Non-Exos + antagomir-708-5p and analysis of ALP activity with ImageJ. (i,j) ARS staining of human BMSCs treated with PBS, Non-Exos, or Non-Exos + antagomir-708-5p and calculation of the area of mineralization with ImageJ. Statistical data are presented as means ± SD from three independent experiments. *$p < 0.05$, **$p < 0.01$, ***$p < 0.001$, and ****$p < 0.0001$.

osteogenic-related protein increased in the hydrogel@antagomiR-708-5p-treated group compared to the other two groups, while interestingly, the hydrogel-treated group also displayed partly overexpression of osteogenic-related protein compared to the control group, but with the same treatment, microCT and HE&Alcian blue staining results did not identify significant differences (Figure 7e,g–k). Therefore, the hydrogel was not shown to promote osteoblast differentiation of BMSCs. The X-ray visualized the dynamic process of fracture healing on days 7, 14, and 21 (Figure 7f). We further carried out microCT on days 14 and 21, and the hydrogel@antagomiR-708-5p group showed higher BV/TV (%) and Tb.Th (mm) than the other two groups (Figure 7g–i). Hematoxylin and eosin (H&E) staining and Alcian blue staining were performed on day 21 post-surgery, the results showed a larger area of bone and smaller area of the cartilage in the hydrogel@antagomiR-708-5p-treated group (Figure 7j,k). In the fracture model with *S. aureus* infection, western blotting

https://doi.org/10.1021/acsami.2c08491
ACS Appl. Mater. Interfaces 2022, 14, 34427–34442

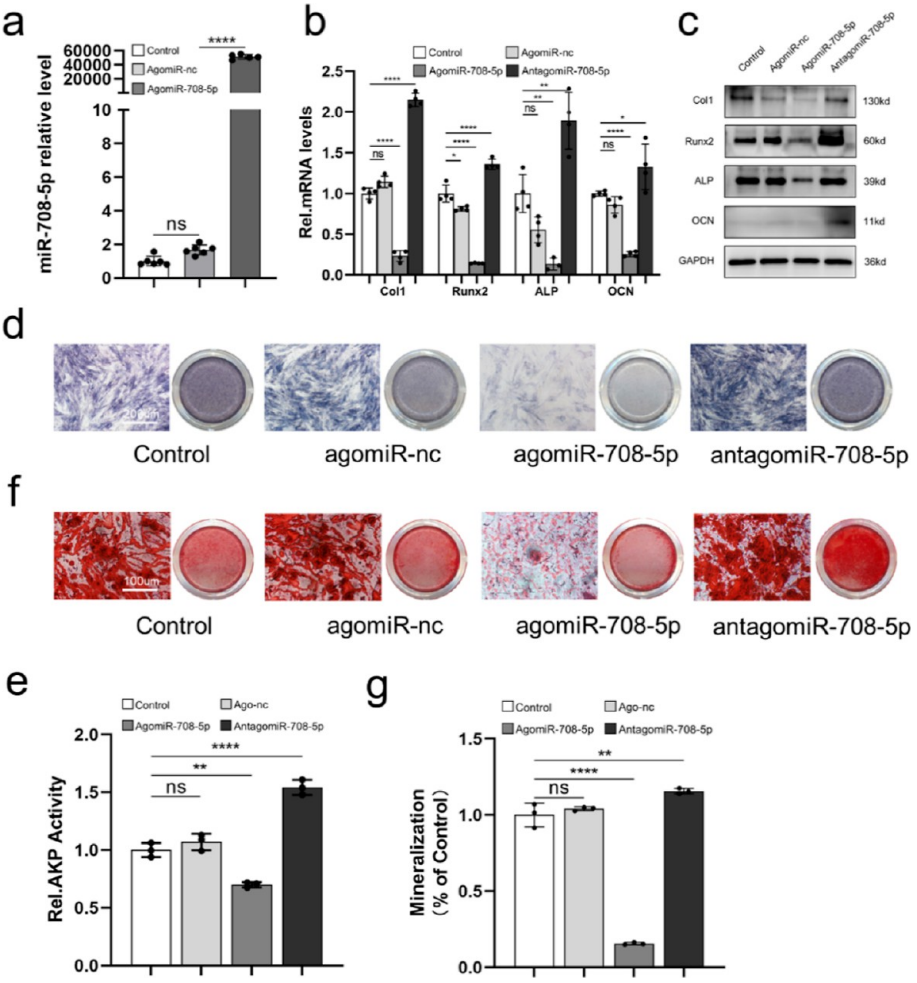

Figure 5. miR-708-5p inhibits osteoblast differentiation of BMSCs. (a) PCR analysis of the miR-708-5p level in BMSCs treated with PBS, agomiR-nc, or agomiR-708-5p. (b,c) PCR and western blot analysis of the mRNA expression levels of Col1, Runx2, ALP, and osteocalcin in BMSCs treated with PBS, agomiR-nc, agomiR-708-5p, or antagomir-708-5p. (d,e) ALP staining of human BMSCs treated with PBS, agomiR-nc, agomiR-708-5p, or antagomir-708-5p and analysis of ALP activity with ImageJ. (f,g) ARS staining of human BMSCs treated with PBS, agomiR-nc, agomiR-708-5p, or antagomir-708-5p and calculation of the area of mineralization with ImageJ. Statistical data are presented as means ± SD from three independent experiments. $*p < 0.05$, $**p < 0.01$, $***p < 0.001$, and $****p < 0.0001$.

showed increased expression of the osteogenic associated protein in the hydrogel or hydrogel@antagomiR-708-5p-treated group, but the latter group showed a greater increase (Figure 7e). X-ray and MicroCT revealed that the fracture model infected with *S. aureus* resulted in a fracture site with no bone formation while the two sides formed a large callus (Figure 7f,g). Fracture healing in the hydrogel-treated group was similar to normal fracture healing with continuous callus formation and a higher level of BV/TV and Tb.Th (mm) than the infected group without treatment, and the hydrogel@antagomiR-708-5p displayed a higher level of BV/TV (%) and Tb.Th (mm) relative to the hydrogel-treated group (Figure 7g–i). The HE&Alcian staining results showed that in the control group, there was normal bone and cartilage formation at the fracture site. In the hydrogel group, there were visible cartilaginous remains (Figure 7j). Compared to the hydrogel-treated group, the hydrogel@antagomiR-708-5p-treated group had a significantly reduced cartilage area and increased bone area (Figure 7k). These results showed that hydrogel@antagomiR-708-5p can accelerate fracture healing with or without *S. aureus* infection, but the therapeutic effects are remarkable for infected fracture healing.

3. DISCUSSION

Limited osteogenesis and inflammation are key components of infected fracture nonunion. In this study, we show that Non-Exos delayed the healing of murine femur fractures. Furthermore, we find that the delayed fracture healing is partly reversed by exosome-derived miR-708-5p. Mechanistically, miR-708-5p targets SSRP1 and therefore inhibits the Wnt/β-catenin signaling pathway. Furthermore, we show the significant therapeutic effects of antibacterial HA hydrogel preloaded with antagomir-708-5p. Collectively, our study underlines the role of exosomes enriched with miR-708-5p in infected fracture nonunion and identifies a promising prevention and treatment strategy for infected fracture nonunion: antibacterial HA hydrogel with miRNA inhibitor release.

BMSCs have significant potential to differentiate into osteoblasts and, hence, promote fracture healing.[28] Recent studies have shown that BMSCs derived from fracture nonunion patients have low osteogenic marker expression and impaired osteogenic differentiation, which partly accounts for the delayed fracture union.[22,29] However, the potential mechanism underlying impaired osteogenesis remains unclear.

https://doi.org/10.1021/acsami.2c08491
ACS Appl. Mater. Interfaces 2022, 14, 34427−34442

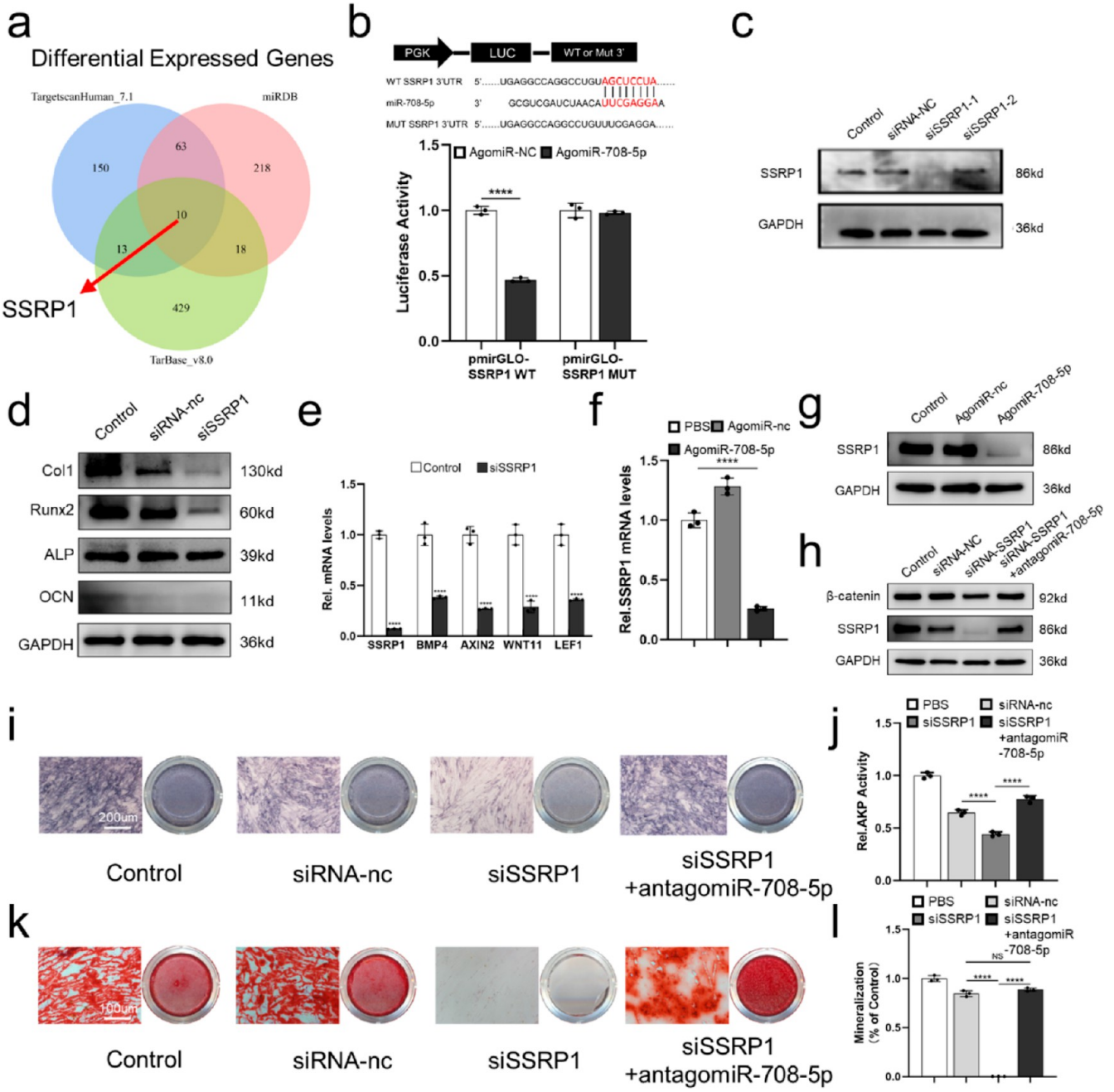

Figure 6. miR-708-5p targets SSRP1 to inhibit osteogenesis of BMSCs by regulating Wnt/β-catenin signaling. (a) Venn diagram of the predicted target genes of miR-708-5p. (b) Relative luciferase activity of HEK293T with pmirGLO-SSRP1 WT or pmirGLO-SSRP1-MUT (Promega) 24 h post-transfection with agomiR-nc or agomiR-708-5p (GenePharma, Shanghai, China). (c) Western blot analysis of siSSRP1 knockdown efficiency in BMSCs after transfection with PBS, siRNA-nc, or siSSRP1-1, siSSRP1-2. (d) Western blot analysis of the protein expression levels of Col1, Runx2, ALP, and osteocalcin in BMSCs transfected with PBS, siRNA-nc, or siSSRP1-1. (e) PCR analysis of the Wnt signaling pathway factor BMP4, AXIN2, Wnt11, and LEF1 mRNA expression in BMSCs after transfection with siRNA-nc or siSSRP1-1. (f) PCR analysis of SSRP1 mRNA expression after transfection with PBS, agomiR-nc, or agomiR-708-5p. (g) Western blot analysis of the protein expression levels of SSRP1 in BMSCs transfected with PBS, agomiR-nc, or agomiR-708-5p. (h) Western blot analysis of the protein expression levels of SSRP1 and β-catenin in BMSCs after transfection with PBS, siRNA-nc, siSSRP1, or siSSRP1 + antagomiR-708-5p. (i,j) ALP staining of BMSCs transfected with PBS, siRNA-nc, siSSRP1, or siSSRP1 + antagomiR-708-5p and analysis of ALP activity with ImageJ. (k,l) ARS staining of BMSCs transfected with PBS, siRNA-nc, siSSRP1, or siSSRP1 + antagomiR-708-5p and calculation of the area of mineralization with ImageJ. Data are presented as means ± SD from three independent experiments. *$p < 0.05$, **$p < 0.01$, ***$p < 0.001$, and ****$p < 0.0001$.

Exosomes, a type of nanoparticles, have been reported to be involved in intercellular communication.[15] The proteins and RNA encapsulated in exosomes are able to maintain normal physiological activity and regulate the physiological functions of receptor cells.[15] Exosomes from multiple types of cells, including macrophages, osteoclasts, endothelial cells, and BMSCs, among others, participate in the osteoblast differentiation of BMSCs under different pathological conditions.[30−33] Additionally, El-Jawhari et al. propose that the serum from fracture nonunion patients might prohibit

https://doi.org/10.1021/acsami.2c08491
ACS Appl. Mater. Interfaces 2022, 14, 34427−34442

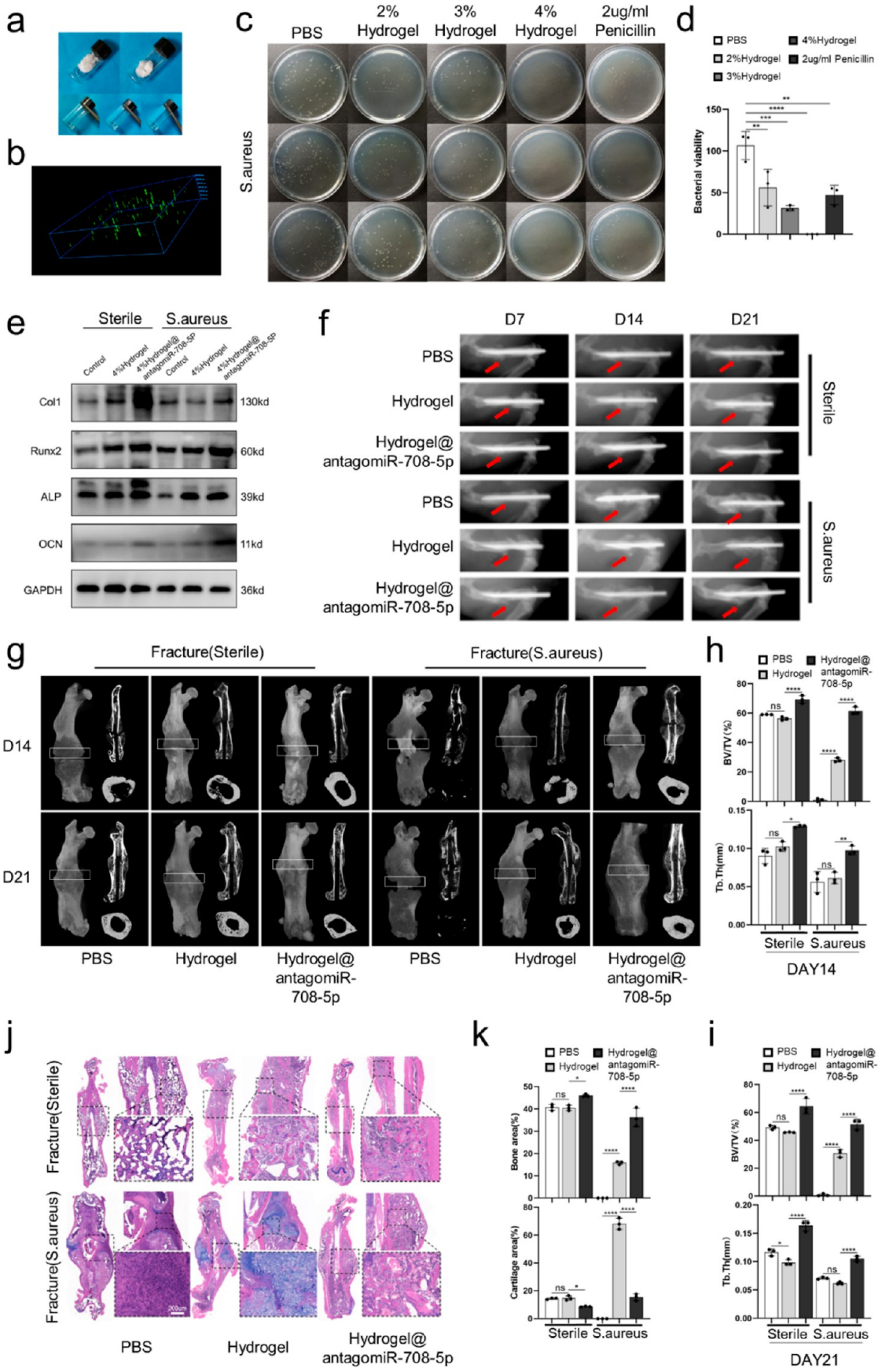

Figure 7. Antibacterial hydrogel preloaded with antagomiR-708-5p applied for the treatment of infected nonunion fractures. A mouse model with a middle femur fracture and stable internal fixation was created in 60 mice. Thirty mice received a local injection of *S. aureus* directly to the fracture site and were equally split into three groups (n = 10 per group) treated with 20 μL of PBS, 20 μL of hydrogel, 20 μL of hydrogel@antagomiR-708-

https://doi.org/10.1021/acsami.2c08491
ACS Appl. Mater. Interfaces 2022, 14, 34427−34442

Figure 7. continued

5p. All the three treatments were locally administered to the fracture site once daily for 3 days until sacrifice. The remaining 30 mice were separated into three equal groups that received the same treatment as above but were not exposed to *S. aureus*. (a) Imaging of HA-ADH plus QA plus aldehyde HA (HA−QA-ALD) hydrogel from solid to solution to hydrogel formation with 1:1 mixing. (b) Confocal imaging of FAM-labeled antagomiR-708-5p distribution on the antibacterial hydrogel. (c,d) Assessment of the antimicrobial properties of the hydrogels. Bacteria were incubated with 2, 3, or 4% of hydrogel and 2 μg/mL penicillin for 2 h at 37 °C, followed by application of the bacterial solution to an agar plate for 16 h and measurement of colony formation. (e) Western blot analysis of the protein expression levels of Col1, Runx2, ALP, and osteocalcin in bone callus from the femurs of a fracture model. (f) Representative images of the fracture sites were assessed by in vivo FX PRO imaging (BRUKER, Karlsruhe, Germany) on day 7, 14, and 21 post-surgery. (g) MicroCT imaging of femurs harvested from mice on day 14 and 21 post-surgery. White box indicating the ROI in the analysis of microCT. (h,i) Evaluation of microCT parameters (BV/TV, Tb.Th) of the bone callus from four different groups of mice (n = 3). (j) HE and Alcian blue staining of femurs harvested from mice on day 21 post-surgery. (k) Assessment of the area of bone and cartilage in the bone callus of mice at day 21 post-surgery calculated with ImageJ software. Data are presented as means ± SD from three independent experiments. *p < 0.05, **p < 0.01, ***p < 0.001, and ****p < 0.0001.

osteogenic differentiation of BMSCs.[22] Hence, we hypothesized that plasma-derived exosomes may be involved in fracture nonunion. Exosomes were purified from plasma via an ultracentrifugation assay and confirmed with TEM, NanoFCM, and western blot. DIR-labeled exosomes were demonstrated in vivo with an FX PRO imaging system. Radiography and pathology revealed that Non-Exos inhibit fracture healing in vivo. Western blot analysis of bone callus showed that Non-Exos reduced the expression of the osteogenic-related proteins Runx2, Col1, ALP, and OCN. PKH26-labeled exosomes could be taken up by human BMSCs, with the BMSCs displaying decreased alkaline phosphatase activity, calcium nodule formation, and expression of osteogenic-related proteins, compared to the control group. All results appear to support the hypothesis that Non-Exos inhibit osteoblast differentiation in BMSCs. The inhibitory effects partly mediated the delayed fracture healing in mice. Based on these in vitro and in vivo results, we hypothesized that Non-Exos may have promising potential to treat fracture nonunion. For this reason, we further explored the mechanisms of action of Non-Exos. Recent pre-clinical experiments have established that miRNAs play an important role in the regulation of fracture healing and their easy application as agonists, and antagonists make them promising therapies for fracture nonunion.[34] Therefore, we performed UID miRNA-seq to identify differentially expressed miRNAs in Non-Exos and NC-Exos. MiR-590-5p and miR-708-5p were shown to be significantly upregulated in Non-Exos. We found that agomiR-708-5p inhibits osteogenesis as shown on ALP staining, but agomiR-708-5p did not significantly impact the ALP activity of BMSCs. A recent study suggested that miR-708-5p is involved in the progression of osteoporosis, therefore also implying the importance of miR-708-5p in the development of bone-related disease. Therefore, we carried out western blotting, ALP staining, and ARS to show that antagomiR-708-5p could partly reverse the inhibitory effects of Non-Exos on osteoblast differentiation, identifying that the Non-Exos inhibitory effects on osteoblast differentiation of BMSCs were partly mediated by miR-708-5p. Exosome-derived microRNAs are taken up by target cells along with exosomes and exert physiological activities within the cells by binding to the corresponding mRNA 3′ non-coding region and downregulating the expression of target mRNA.[21] To further verify the value of miR-708-5p, we used bioinformatic tools to predict miR-708-5p target genes, whose results are represented in Figure 6a. The histone chaperone that facilitates chromatin transactions (FACT) is composed of two subunits, SSRP1 and SPT16, and is involved in DNA transcription, replication, and repair.[35] Studies show that FACT is associated with the induction of pluripotency.[36−38] SSRP1 has been reported to be essential for the activity of the Wnt signaling pathway during osteoblast differentiation. In the past few decades, the Wnt/β-catenin signaling pathway has been identified as essential for bone formation and is involved in amino acid, lipid, and glucose metabolism in bone tissue.[39,40] β-Catenin is indispensable for bone formation and participates in various stages of osteoblast differentiation.[49−53] We found that miR-708-5p was able to interact with the non-coding region at the 3′ end of SSRP1 mRNA and inhibit the expression of SSRP1. AntagomiR-708-5p partly reverses the adverse effects of SSRP1 inhibition on Wnt/β-catenin signaling activity and osteoblast differentiation.

These findings emphasize the key role of miR-708-5p in the pathological process of fracture nonunion and highlight the potential value of antagomiR-708-5p as a therapy of fracture nonunion. Infection is a critical cause of delayed healing or nonunion.[2] As the Orthopedic Trauma Association Open Fracture Classification describes, the incidence of FRI is up to 25% depending on the severity of the trauma for a patient with open fracture.[41−43] Therefore, the prevention and treatment of FRI are essential for minimizing fracture nonunion.[44] Though FRI is associated with several microorganisms, *S. aureus* is the most common pathogenic bacterium.[28, 58] To evaluate the efficacy of antagomiR-708-5p in fracture nonunion, we established an infected fracture nonunion model by seeding a femur fracture site in mice with *S. aureus*. In a previous study, our team synthesized a multifunctional HA hydrogel using positively charged QA, which displayed excellent anti-inflammatory properties. We found that HA hydrogel preloaded with antagomiR-708-5p had a significant anti-inflammatory effect and accelerated fracture healing in mice. Our finding provided an outstanding therapeutic strategy for fracture nonunion.

Furthermore, to better understand the pathological mechanisms underlying infected fracture nonunion and develop better treatments to reduce the rate of fracture nonunion, we investigate exosomes. The inflammatory response leads to local recruitment of macrophages, which although essential for fracture healing, long-term chronic inflammatory responses can impair fracture healing.[45] Our previous study found that M1-type macrophage-derived exosomes inhibit osteogenic differentiation of BMSCs.[46] We therefore considered whether exosomes enriched with miR-708-5p from the peripheral blood of patients with infected fracture nonunion were macrophage derived. In this study, we co-cultured *S. aureus* with macrophages and isolated the exosomes from the culture medium. qPCR revealed increased expression of miR-708-5p

https://doi.org/10.1021/acsami.2c08491
ACS Appl. Mater. Interfaces 2022, 14, 34427−34442

in exosomes secreted by *S. aureus* co-cultured macrophages. We found that *S. aureus* co-cultured macrophage-derived exosomes inhibited the expression of BMSC osteogenic-related proteins, osteogenic differentiation, and calcium nodule formation in BMSCs. The results of the in vitro experiments demonstrated that exosomes with high miR-708-5p expression from the peripheral blood of patients with infected fracture nonunion may be derived from macrophages. Although the evidence toward the source of exosomes is insufficient, it still identifies that the bone marrow immune microenvironment plays an important role in infected fracture nonunion and warrants further investigation.

4. CONCLUSIONS

Taken together, our results indicate that plasma exosomes isolated from patients with infected fracture nonunion could delay fracture repair via inhibition of osteoblast differentiation of BMSCs in vitro and in vivo. The effect could be partially mediated with miR-708-5p. Mechanistically, miR-708-5p inhibits osteogenic differentiation of the BMSCs by targeting SSRP1 and suppressing the wnt/β-catenin signaling pathway. Antibacterial hydrogel preloaded with antagomiR-708-5p largely accelerated fracture healing via promotion of osteoblast differentiation and anti-inflammation. Therefore, antibacterial hydrogel preloaded with antagomiR-708-5p appears to be a promising tool for prevention and therapy of infected fracture nonunion.

5. MATERIALS AND METHODS

5.1. Exosome Isolation and Identification. Blood was collected in ethylenediaminetetraacetic acid-containing tubes from male volunteers aged 20−60 years old who were diagnosed with fracture non-healing (n = 3) or healing (n = 3) at Union Hospital, Tongji Medical College, Huazhong University of Science and Technology. This study was approved by the Ethics Committee of Union Hospital, Tongji Medical College, Huazhong University of Science and Technology. The blood samples were centrifuged at 3000 rpm for 15 min at room temperature (RT) and transferred to 2 mL lyophilization tubes. The isolated plasma was kept at −80 °C temporarily. Exosome purification, identification, and quantification were performed as previously described.[47] Briefly, rapidly melted plasma was resuspended in PBS after several cycles of ultracentrifugation, washing, and filtration. Exosomes were stained with 1% phosphotungstic acid and imaged with TEM (FEI Tecnai Spirit TEM T12). Information on particle size and concentration of the exosomes was detected with a NanoFCM instrument (Flow Bio Flow NanoAnalyzer). Western blotting was performed to assess the expression of exosomal surface markers. Individual exosomes were used in different experiments.

5.2. Preparation of the HA Hydrogel and HA Hydrogel@antagomiR-70-5p. Synthesis of HA-ADH, QA, and aldehyde HA (HA−QA-ALD) was conducted as described in a previous study.[23] The HA hydrogel was obtained by mixing HA-ADH and HA−QA-ALD solution at a ratio of 1:1 using a handmade dual syringe. HA hydrogel@antagomiR-70-5p synthesis was conducted by mixing HA-ADH with FAM-tagged antagomiR-708-5p and HA−QA-ALD at a ratio of 1:1. The distribution of antagomiR-708-5p was imaged using a confocal microscope. The final solid content was used to differentiate each HA hydrogel group; for example, 4% HA hydrogel was made by mixing 4% HA-ADH and 4% HA−QA-ALD.

5.3. *S aureus* Culture and Antibiotic Activity of the Hydrogel. For bacterial culture, *S. aureus* was kindly donated by the Department of Orthopaedics, Union Hospital, Tongji Medical College, Huazhong University of Science and Technology. Frozen *S. aureus* was rapidly transferred from the refrigerator to a constant temperature water bath at 37 °C. LB powder (PM0010, Cooler, Beijing, China) was dissolved in 500 mL of ddH_2O (pH 7.2−7.4) and sterilized for *S. aureus* culture. Culture flasks, containing *S. aureus*, were placed in a water bath shaker at 37 °C and incubated overnight. Macrobid tubes (Solarbio, YA0180, Beijing, China) were used for bacterial quantification. For the hydrogel antibiotic activity test, a 48-well plate was prepared and pretreated with PBS; 2, 3, or 4% HA hydrogel; and 2% penicillin. Then, 30 μL of 3×10^5 CFU/mL *S. aureus* was added to each well and incubated for 2 h at 37 °C. After a certain dilution, the bacterial solution from each well was evenly spread onto a pre-prepared LB solid medium (1% agar), and the number of bacterial colonies was counted after 16 h.

5.4. Animal Fracture Model. Fracture models with or without *S. aureus* infection were created as previously described.[48,49] Male C57BL/6J mice (n = 90; aged 8 weeks) were purchased from Speford Biotechnology Company (Beijing, China). All experiments were performed according to the guidelines of the Animal Care and Use Committee at Tongji Medical College, Huazhong University of Science and Technology. Anesthesia was performed with 1% pentobarbital (1 mg/10 g body weight). An electric pusher was used to expose the skin covering the surface of the femur and the surrounding area. The 0.5% iodophor was used to disinfect the surgical area. The skin was cut along the long axis of the femur with sterile tissue scissors. The muscle was bluntly separated with ophthalmic forceps to expose the mid-femur. For the sterile fracture model, femoral shaft transverse fracture was performed with a water-port clamp. Internal fixation of the fracture of the femoral shaft was done with 0.6 mm intramedullary needles. In the infected group, 5 μL of PBS containing 1×10^6 CFU *S. aureus* was applied to the fracture site. Ten minutes later, sterile gauze was used to absorb the fluid in the fracture site. A third of the mice were sacrificed on the 10th postoperative day for callus harvesting. The remaining mice were executed 14 or 21 days after surgery for microCT and H&E or Alcian blue staining.

5.5. Treatments of the Fracture. To explore the negative effects of circulating exosomes from the bone nonunion patients, we applied PBS, 50 μg/mL control exosomes, and 50 and 100 μg/mL exosomes from patients with bone nonunion twice to the fracture sites of the mice (n = 10) once every 3 days for 2 weeks post-surgery. To explore the therapeutic effects of hydrogel@antagomiR-708-5p, mice, with or without *S. aureus*, were treated with local administration of PBS, 4% hydrogel, or 4% hydrogel@antagomiR-708-5p twice a week for 2 weeks post-surgery.

5.6. Exosomes In Vivo Fluorescence Imaging. DIR dye (AAT Bioquest, Inc., 22070, America) was used to label the exosomes. The DIR dye (25 mg) was dissolved in 10 mL of sterile dimethyl sulfoxide (Sigma, D2650-5, USA). The DIR dye (2.5 μg/mL) was incubated with exosomes for 10 min, shielded from light. The supernatant was removed by centrifugation at 100,000g for 1 h, and the exosomes were resuspended in PBS (50 or 100 μg/mL). The DIR dye-tagged exosomes were administered to the fracture site. One day later, the exosome-treated mice were investigated with an in vivo FX PRO imaging system (BRUKER, Karlsruhe, Germany) for X-ray and fluorescence imaging (Ex/Em = 750/790 nm) under anesthesia. Bruker MI SE 7.2 software was used to process the imaging.

5.7. Radiographic Imaging. The process of fracture healing was observed with the Vivo FX PRO imaging system (BRUKER, Karlsruhe, Germany) after anesthetizing mice with 1% pentobarbital on days 7, 14, and 21 after surgery. The exposure time was set to 30 s. Bruker MI SE 7.2 software was used for analysis.

5.8. MicroCT. Mice were sacrificed on day 14 (n = 3) or day 21 (n = 3), and the femurs and soft tissue were harvested. The bones were fixed with 4% paraformaldehyde overnight and scanned using the BRUKER SkyScan 1176 scanner mCT system with the following settings: 2,400 views, five frames/view, 37 kV, and 121 mA. Reconstructed (3D) images were generated using CT-Vox 2.1 version (BRUKER Minimal Intensity Projection Software, Karlsruhe, Germany) and Dataviewer. Parameters including BV over TV (BV/TV) and Tb.Th were measured and analyzed with CTAN 1.12 version (BRUKER Minimal Intensity Projection Software, Karlsruhe,

https://doi.org/10.1021/acsami.2c08491
ACS Appl. Mater. Interfaces 2022, 14, 34427−34442

Table 2. miRNAs and mRNA Primer Sequences

microRNAs or gene name	primer sequence (5′ to 3′)
hsa-miR-708-5p-reverse	GTCGTATCCAGTGCAGGGTCCGAGGTATTCGCACTGGATACGACCCCACC
hsa-miR-708-5p-forward	CGGGCAAGGAGCTTACAA
hsa-miR-reverse	GTGCAGGGTCCGAGGT
hsa-ALP-forward	ACTGGGGCCTGAGATACCC
hsa-ALP-reverse	TCGTGTTGCACTGGTTAAAGC
hsa-COL1A1-forward	GAGGGCCAAGACGAAGACATC
hsa-COL1A1-reverse	CAGATCACGTCATCGCACAAC
hsa-OCN-forward	GGCGCTACCTGTATCAATGG
hsa-OCN-reverse	GTGGTCAGCCAACTCGTCA
hsa-Runx2-forward	TGGTTACTGTCATGGCGGGTA
hsa-Runx2-reverse	TCTCAGATCGTTGAACCTTGCTA
hsa-U6-forward	AGCACATATACTAAAATTGGAACGAT
hsa-U6-reverse	GTCGTATCGACTGCAGGGTCCGAGGTATTCGCAGTCGATACGACAAAATATG
hsa-AXIN2-forward	ATTTCCCGAGAACCCACCGCCT
hsa-AXIN2-reverse	GGCTGTGGCGGCTCTCCAAC
hsa-BMP4-forward	GGAGCTTCCACCACGAAGAA
hsa-BMP4-reverse	GGAAGCCCCTTTCCCAATCA
hsa-LEF1-forward	GACGAGATGATCCCCTTCAA
hsa-LEF1-reverse	CGGGATGATTTCAGACTCGT
hsa-Wnt11-forward	GCCAAGTTTTCCGATGCTCC
hsa-Wnt11-reverse	GACACCCCATGGCACTTACA
hsa-SSRP1-forward	AAAGGTTCCATGAATGATGGTC
hsa-SSRP1-reverse	GCCTGGATGTTGTCCACTTT
hsa-GAPDH-forward	CCGTTGAATTTGCCGTGA
hsa-GAPDH-reverse	TGATGACCCTTTTGGCTCCC

Germany). The bones were then sent for H&E staining and Alcian blue staining.

5.9. Histological Analysis. After completion of the CT scan, the femurs were placed in a decalcification fluid (Servicebio, G1105-500ML, Wuhan, China) for three consecutive weeks, with the decalcification fluid being changed every 3 days. The decalcified femur was embedded with paraffin and sectioned in the direction of the long axis of the femoral stem with a thickness of 5 μm. The sections were fixed on the slides and stained with H&E and Alcian blue. The sections were imaged with an Olympus BX51 microscope and a DP73 CCD Olympus Imaging System (Olympus Corporation, Tokyo). Caseviewer 2.4 (3DHISTECH Ltd, Hungary) was used to observe and analyze the morphology of the specimens at 0.8×, 5×, and 20× magnifications. ImageJ was used to calculate the area of bone and cartilage of the callus.

5.10. Cell Culture, Transfection, and Differentiation. Human bone marrow specimens were harvested from young volunteers (<22 years old). BMSC isolation was operated according to the instruction manual of the human lymphocyte separation medium (TBD, LTS1077, Tianjin, China). DMEM/F12 medium (GIBCO, C11330500BT, Shanghai, China) containing 10% fetal bovine serum (GIBCO, 10099-141, Australia) and 1% penicillin−streptomycin solution were used to culture BMSCs with medium replacement every 3 day at 37 °C in an incubator with 5% CO_2 and 95% humidity. Identification of BMSCs was done as described.[50] The third passage cells were used for subsequent experiments. AgomiR-708-5p, antagomiR-708-5p, agomiR-590-5p, and agomiR-negative control were purchased from GenPharma (Suzhou, China). siRNA-SSRP1-1 and siRNA-SSRP1-2 siSSRP1-NC were purchased from Tsingke Biotechnology Co., Ltd. (Wuhan, China). AgomiRNA, antagomiRNA, and siRNA transfection was done with the Lipofectamine 3000 reagent (Invitrogen, L3000015, Carlsbad, CA) according to the manufacturer's manuals. Cells were harvested after 48 h for qPCR or 96 h for western blotting to verify the effects of transfection. Human bone marrow mesenchymal stem cell differentiation induction medium (Cyagen, HUXMA-90021, Guangzhou, China) was used for inducing BMSC osteogenic differentiation.

5.11. Exosomes Uptake. BMSCs were inoculated in confocal dishes until the fusion was approximately 30%. Different groups of serum-derived exosomes were labeled with PKH26 red fluorescent (Sigma, MKCH0526) according to the manufacturer's manual. The FITC-labeled exosomes were added to the confocal dishes containing the prepared BMSCs and co-incubated for 8 h protected from light in an incubator at 37 °C. The cell supernatant was removed, and the cells were washed three times with PBS. The cells were fixed in 4% paraformaldehyde for 10 min in the dark and washed with PBS three times. The cytoskeleton and nucleus were stained with phalloidin (Solarbio, CA1620, Beijing, China). An antifluorescence quenching agent (Solarbio, S2100, Beijing, China) was added to the confocal dishes, and the dishes were visualized under a confocal microscope.

5.12. UID miRNA-Seq. miRNA library preparation, high-throughput sequencing, and miRNA-seq data analysis were performed by Seqhealth Technology Co., LTD (Wuhan, China). The miRNA library was prepared using the NEBNext Multiplex Small RNA Library Prep Set for Illumina (catalog no. E7300, New England Biolabs) following the manufacturer's protocol. A unique molecular identifier (Seqhealth Technology Co., LTD) was used to label the pre-amplified small RNA molecules. RNA library purification was performed by using 6% polyacrylamide gel electrophoresis gel. The library quantification was finished by using a QubitTM3 fluorometer (Invitrogen, cat. no. Q33216) with Qubit dsDNA HS Assay Kit (Invitrogen, cat. no. Q32854). The library examination was undertaken by using the Qsep100TM bio-fragment analyzer (Bioptic Inc., Taiwan, China). The RNA library on Novaseq 6000 sequencer (Illumina) was visualized with a PE150 model. Raw sequencing data filtration was carried out to remove the low-quality reads by fastx_toolkit (version: 0.0.13.2), and the cutadapt (version: 1.15) was used to shear the adaptor sequences. The processed reads were treated to diminish duplication bias.

5.13. RT-PCR and Real-Time PCR. The total RNA in cells was isolated and purified with the RNAiso reagent (Takara,9109, Japan). Chloroform, isopropanol, and anhydrous ethanol were used for purification as per the previous literature. miRNA purification was performed with an miRNA Purification Kit (Cwbio, CW0627, Jiangsu Province, China) according to the manufacturer's instructions.

https://doi.org/10.1021/acsami.2c08491
ACS Appl. Mater. Interfaces 2022, 14, 34427−34442

Nanodrop 2000 (Thermo Scientific, MA, United States) was used for mRNA or miRNA quantification. mRNA or miRNA (1 μg) per sample was used for RT-PCR. We obtained cDNA using the HiScript III-RT SuperMix for qPCR (Vazyme, R323-01, Nanjing, China) and synthesized has-miRNA-708-5p reverse transcription products using the miRNA 1st strand cDNA Synthesis Kit (by stem-loop) (Vazyme, MR101-01/02, Nanjing, China). Primers for mRNA, miRNA, and U6 were purchased from Tsingke Biotechnology Co., Ltd. (Wuhan, China). For real-time PCR, the reaction system preparation and the reaction program setting were carried out as per the manufacturer's manual of the AceQ qPCR SYBR Green Master Mix (Vazyme, Q111-C1, Nanjing, China). Finally, real-time PCR was performed by using a Bio-rad CFX96 system. miRNAs and mRNA primer sequences are listed (Table 2).

5.14. Western Blot Analysis. Bone tissues were placed in a mortar, and liquid nitrogen was added, allowing the callus to be ground to fine particles with a pestle. Subsequently, the tissue was transferred to a 1.5 mL EP tube for protein isolation. Total protein was extracted from cells and tissues by RIPA (Beyotime, P0013B, Shanghai, China) with 1% protease inhibitor cocktail for general use, 100× (Beyotime, P1005, Shanghai, China). Protein (20 μg) was separated on a denatured sodium dodecyl sulfate-polyacrylamide gel and transferred to a polyvinylidene fluoride (PVDF) membrane. The PVDF membrane was blocked with defat mike (5% dissolved in TBS-T) for 2 h and then incubated with rabbit polyclonal ALP (1:1000, Abcam), Runx2 (1:1000, Abclonal), OCN (1:500, Abcam), collagen I (Col1) (1:3000, Abcam), GAPDH (1:1000, Abclonal), SSRP1 (1; 1000, Proteintech), and β-catenin (1:1000, Abclonal) for 16 h at 4 °C. After being washed three times, the membranes were followed by incubation with horseradish peroxidase-coupled goat antirabbit IgG H&L for 1 h at 37 °C. The blotting membrane was treated with an ECL chemiluminescent substrate (Biosharp, BL520A, Shanghai, China) and visualized using a ChemiDoc MP chemiluminescence gel imaging system (Bio-Rad,1708280, California, USA).

5.15. ARS and ALP Staining. BMSCs, third to fourth generation, were seeded into 24-well plates pre-coated with 0.1% gelatin. After treatment, when cell fusion reached 60−70%, the human bone marrow MSC osteogenic differentiation induction medium was changed every 3 days (Cyagen, HUXMA-90021, Guangzhou, China), and osteogenic differentiation induction was started. ARS was performed 21 days later. When obvious calcium nodules were observed in the control group, the cell medium was removed. The cells were washed three times with PBS, fixed with 4% paraformaldehyde, washed three times with PBS, and then stained with ARS solution for 3−5 min. For ALP staining, after 7 days, alkaline phosphatase dye was pre-configured in advance according to the manufacturer's instructions by using the BCIP/NBT alkaline phosphatase chromogenic kit (Beyotime, C3206, Shanghai, China). The cells were first fixed in 4% paraformaldehyde, washed three times in PBS, and incubated for 30 min with the dye protected from light. The cells were washed three times with PBS and placed under a microscope and a camera for photography.

5.16. Luciferase Reporter Assay. The duel-luciferase vectors were constructed by cloning the 3′-UTR sequence of the predicted complementary fragment or the mutated SSRP1 sequence into the pmir-GLO-promoter vector (Promega). HEK293T cells were incubated in 24-well plates (2.5×10^5 cell/well), followed by transfection with the constructed dual-luciferase vectors (pmirGLO-SSRP1 WT and pmirGLO-SSRP1-MUT) along with either Hsa-miR-708-5p agonist (AgomiR-708-5p, GenePharma, Shanghai, China) or negative control (AgomiR-nc, GenePharma, Shanghai, China) according to the lipo3000 (Thermo Fisher) manufacturer's instructions. After 24 h of transfection, the luciferase activity was measured following the instructions of the Dual-Lucy Assay Kit (Solarbio, China). Ultimately, the firefly luciferase activity was normalized to the paired Renilla luciferase signaling activity.

5.17. Statistical Analysis. Graphical data were presented as means ± standard deviation (SD). Statistical significance of differences between groups was assessed with one-way ANOVA for three groups or Student's *t*-test for two groups analyzed with GraphPad Prism 8.0 (GraphPad Software, Inc, La Jolla, CA). A value of $p < 0.05$ was considered statistically significant.

■ ASSOCIATED CONTENT

Supporting Information

The Supporting Information is available free of charge at https://pubs.acs.org/doi/10.1021/acsami.2c08491.

Effect of MD-bExos on osteogenesis of BMSCs; biocompatibility and bactericidal effect of HA hydrogel; and release profile of FAM-antagomiR-708-5p from HA hydrogels (PDF)

■ AUTHOR INFORMATION

Corresponding Authors

Bobin Mi − *Department of Orthopaedics, Union Hospital, Tongji Medical College, Huazhong University of Science and Technology, Wuhan 430022, China; Hubei Province Key Laboratory of Oral and Maxillofacial Development and Regeneration, Wuhan 430022, China*; Email: mibobin@hust.edu.cn

Guohui Liu − *Department of Orthopaedics, Union Hospital, Tongji Medical College, Huazhong University of Science and Technology, Wuhan 430022, China; Hubei Province Key Laboratory of Oral and Maxillofacial Development and Regeneration, Wuhan 430022, China*; orcid.org/0000-0002-2013-1396; Email: liuguohui@hust.edu.cn

Authors

Chenyan Yu − *Department of Orthopaedics, Union Hospital, Tongji Medical College, Huazhong University of Science and Technology, Wuhan 430022, China; Hubei Province Key Laboratory of Oral and Maxillofacial Development and Regeneration, Wuhan 430022, China*

Lang Chen − *Department of Orthopaedics, Union Hospital, Tongji Medical College, Huazhong University of Science and Technology, Wuhan 430022, China; Hubei Province Key Laboratory of Oral and Maxillofacial Development and Regeneration, Wuhan 430022, China; Department of Physics and Center for Hybrid Nanostructure (CHyN), University of Hamburg, Hamburg 22761, Germany*

Wu Zhou − *Department of Orthopaedics, Union Hospital, Tongji Medical College, Huazhong University of Science and Technology, Wuhan 430022, China; Hubei Province Key Laboratory of Oral and Maxillofacial Development and Regeneration, Wuhan 430022, China*

Liangcong Hu − *Department of Orthopaedics, Union Hospital, Tongji Medical College, Huazhong University of Science and Technology, Wuhan 430022, China; Hubei Province Key Laboratory of Oral and Maxillofacial Development and Regeneration, Wuhan 430022, China*

Xudong Xie − *Department of Orthopaedics, Union Hospital, Tongji Medical College, Huazhong University of Science and Technology, Wuhan 430022, China; Hubei Province Key Laboratory of Oral and Maxillofacial Development and Regeneration, Wuhan 430022, China*

Ze Lin − *Department of Orthopaedics, Union Hospital, Tongji Medical College, Huazhong University of Science and Technology, Wuhan 430022, China; Hubei Province Key Laboratory of Oral and Maxillofacial Development and Regeneration, Wuhan 430022, China*

Adriana C. Panayi − *Division of Plastic Surgery, Brigham and Women's Hospital, Harvard Medical School, Boston, Massachusetts 02215, United States*

Xingjie Zhan − *Tianyou Hospital Affiliated to Wuhan University of Science and Technology, Wuhan 430022, China*
Ranyang Tao − *Department of Orthopaedics, Union Hospital, Tongji Medical College, Huazhong University of Science and Technology, Wuhan 430022, China; Hubei Province Key Laboratory of Oral and Maxillofacial Development and Regeneration, Wuhan 430022, China*

Complete contact information is available at: https://pubs.acs.org/10.1021/acsami.2c08491

Author Contributions

#C.Y., L.C., and W.Z. contributed equally to this work.

Notes

The authors declare no competing financial interest.

■ ACKNOWLEDGMENTS

This study was supported by the National Natural Science Foundation of China (grant nos. 82002313 and 82072444), the Department of Science and Technology of Hubei Province (grant no. 2021CFB425), and the National Key Research & Development Program of China (grant nos. 2021YFA1101503, 2018YFC2001502, and 2018YFB1105705). The authors thank the Huazhong University of Science & Technology Analytical & Testing center, Medical sub-center, for the technical support.

■ REFERENCES

(1) Zura, R.; Xiong, Z.; Einhorn, T.; Watson, J. T.; Ostrum, R. F.; Prayson, M. J.; Della Rocca, G. J.; Mehta, S.; McKinley, T.; Wang, Z.; Steen, R. G. Epidemiology of Fracture Nonunion in 18 Human Bones. *JAMA Surg.* **2016**, *151*, No. e162775.
(2) Mills, L.; Tsang, J.; Hopper, G.; Keenan, G.; Simpson, A. H. R. W. The Multifactorial Aetiology of Fracture Nonunion and the Importance of Searching for Latent Infection. *Bone Joint Res.* **2016**, *5*, 512−519.
(3) Morgenstern, M.; Kühl, R.; Eckardt, H.; Acklin, Y.; Stanic, B.; Garcia, M.; Baumhoer, D.; Metsemakers, W. J. Diagnostic Challenges and Future Perspectives in Fracture-Related Infection. *Injury* **2018**, *49*, S83−S90.
(4) Trampuz, A.; Zimmerli, W. Diagnosis and Treatment of Infections Associated with Fracture-Fixation Devices. *Injury* **2006**, *37* (2 SUPPL.). DOI: DOI: 10.1016/J.INJURY.2006.04.010.
(5) Hogan, A.; Heppert, V. G.; Suda, A. Osteomyelitis. *Arch. Orthop. Trauma Surg.* **2013**, *133*, 1183−1196.
(6) Jiang, N.; Wang, B.-w.; Chai, Y.-m.; Wu, X.-b.; Tang, P.-f.; Zhang, Y.-z.; Yu, B. Chinese Expert Consensus on Diagnosis and Treatment of Infection after Fracture Fixation. *Injury* **2019**, *50*, 1952−1958.
(7) Ferguson, J. Y.; Dudareva, M.; Riley, N. D.; Stubbs, D.; Atkins, B. L.; McNally, M. A. The use of a biodegradable antibiotic-loaded calcium sulphate carrier containing tobramycin for the treatment of chronic osteomyelitis. *Bone Joint J.* **2014**, *96-B*, 829−836.
(8) McNally, M. A.; Ferguson, J. Y.; Lau, A. C. K.; Diefenbeck, M.; Scarborough, M.; Ramsden, A. J.; Atkins, B. L. Single-stage treatment of chronic osteomyelitis with a new absorbable, gentamicin-loaded, calcium sulphate/hydroxyapatite biocomposite. *Bone Joint J.* **2016**, *98-B*, 1289−1296.
(9) Calori, G. M.; Colombo, M.; Mazza, E. L.; Mazzola, S.; Malagoli, E.; Mineo, G. V. Incidence of Donor Site Morbidity Following Harvesting from Iliac Crest or RIA Graft. *Injury* **2014**, *45*, S116−S120.
(10) Lin, K.; VandenBerg, J.; Putnam, S. M.; Parks, C. D.; Spraggs-Hughes, A.; McAndrew, C. M.; Ricci, W. M.; Gardner, M. J. Bone Marrow Aspirate Concentrate with Cancellous Allograft versus Iliac Crest Bone Graft in the Treatment of Long Bone Nonunions. *OTA Int.* **2019**, *2*, No. e012.
(11) Van Vugt, T. A. G.; Geurts, J. A. P.; Blokhuis, T. J. Treatment of Infected Tibial Non-Unions Using a BMAC and S53P4 BAG Combination for Reconstruction of Segmental Bone Defects: A Clinical Case Series. *Injury* **2021**, *52*, S67−S71.
(12) Braly, H. L.; O'Connor, D. P.; Brinker, M. R. Percutaneous Autologous Bone Marrow Injection in the Treatment of Distal Meta-Diaphyseal Tibial Nonunions and Delayed Unions. *J. Orthop. Traumatol.* **2013**, *27*, 527−533.
(13) Deatherage, B. L.; Cookson, B. T. Membrane Vesicle Release in Bacteria, Eukaryotes, and Archaea: A Conserved yet Underappreciated Aspect of Microbial Life. *Infect. Immun.* **2012**, *80*, 1948−1957.
(14) Koniusz, S.; Andrzejewska, A.; Muraca, M.; Srivastava, A. K.; Janowski, M.; Lukomska, B. Extracellular Vesicles in Physiology, Pathology, and Therapy of the Immune and Central Nervous System, with Focus on Extracellular Vesicles Derived from Mesenchymal Stem Cells as Therapeutic Tools. *Front. Cell. Neurosci.* **2016**, *10*, 109.
(15) Kalluri, R.; LeBleu, V. S. The Biology , Function , and Biomedical Applications of Exosomes. *Science* **2020**, *367*, No. eaau6977.
(16) Rupaimoole, R.; Slack, F. J. MicroRNA Therapeutics: Towards a New Era for the Management of Cancer and Other Diseases. *Nat. Rev. Drug Discovery* **2017**, *16*, 203−222.
(17) Hou, X.; Yin, S.; Ren, R.; Liu, S.; Yong, L.; Liu, Y.; Li, Y.; Zheng, M. H.; Kunos, G.; Gao, B.; Wang, H. Myeloid-Cell-Specific IL-6 Signaling Promotes MicroRNA-223-Enriched Exosome Production to Attenuate NAFLD-Associated Fibrosis. *Hepatology* **2021**, *74*, 116−132.
(18) Ying, W.; Gao, H.; Dos Reis, F. C. G.; Bandyopadhyay, G.; Ofrecio, J. M.; Luo, Z.; Ji, Y.; Jin, Z.; Ly, C.; Olefsky, J. M. MiR-690, an Exosomal-Derived MiRNA from M2-Polarized Macrophages, Improves Insulin Sensitivity in Obese Mice. *Cell Metab.* **2021**, *33*, 781−790.
(19) Zhao, J.; Li, X.; Hu, J.; Chen, F.; Qiao, S.; Sun, X.; Gao, L.; Xie, J.; Xu, B. Mesenchymal Stromal Cell-Derived Exosomes Attenuate Myocardial Ischaemia-Reperfusion Injury through MiR-182-Regulated Macrophage Polarization. *Cardiovasc. Res.* **2019**, *115*, 1205−1216.
(20) Wang, C.; Zhang, C.; Liu, L.; A, A.; Chen, B.; Li, Y.; Du, J. Macrophage-Derived Mir-155-Containing Exosomes Suppress Fibroblast Proliferation and Promote Fibroblast Inflammation during Cardiac Injury. *Mol. Ther.* **2017**, *25*, 192−204.
(21) Sun, Z.; Shi, K.; Yang, S.; Liu, J.; Zhou, Q.; Wang, G.; Song, J.; Li, Z.; Zhang, Z.; Yuan, W. Effect of Exosomal MiRNA on Cancer Biology and Clinical Applications. *Mol. Cancer* **2018**, *17*, 147.
(22) El-Jawhari, J. J.; Kleftouris, G.; El-Sherbiny, Y.; Saleeb, H.; West, R. M.; Jones, E.; Giannoudis, P. V. Defective Proliferation and Osteogenic Potential with Altered Immunoregulatory Phenotype of Native Bone Marrow-Multipotential Stromal Cells in Atrophic Fracture Non-Union. *Sci. Rep.* **2019**, *9*, 17340.
(23) Liu, P.; Xiong, Y.; Chen, L.; Lin, C.; Yang, Y.; Lin, Z.; Yu, Y.; Mi, B.; Liu, G.; Xiao, X.; Feng, Q. Angiogenesis-Based Diabetic Skin Reconstruction through Multifunctional Hydrogel with Sustained Releasing of M2 Macrophage-Derived Exosome. *Chem. Eng. J.* **2022**, *431*, 132413.
(24) Zhang, Y.; Bi, J.; Huang, J.; Tang, Y.; Du, S.; Li, P. Exosome: A Review of Its Classification, Isolation Techniques, Storage, Diagnostic and Targeted Therapy Applications. *Int. J. Nanomed.* **2020**, *15*, 6917−6934.
(25) Lässer, C.; Seyed Alikhani, V.; Ekström, K.; Eldh, M.; Torregrosa Paredes, P.; Bossios, A.; Sjöstrand, M.; Gabrielsson, S.; Lötvall, J.; Valadi, H. Human Saliva, Plasma and Breast Milk Exosomes Contain RNA: Uptake by Macrophages. *J. Transl. Med.* **2011**, *9*, 9.
(26) Hossan, T.; Nagarajan, S.; Baumgart, S. J.; Xie, W.; Magallanes, R. T.; Hernandez, C.; Chiaroni, P. M.; Indenbirken, D.; Spitzner, M.; Thomas-Chollier, M.; Grade, M.; Thieffry, D.; Grundhoff, A.; Wegwitz, F.; Johnsen, S. A. Histone Chaperone SSRP1 Is Essential

for Wnt Signaling Pathway Activity During Osteoblast Differentiation. *Stem Cells* **2016**, *34*, 1369−1376.
(27) Depypere, M.; Morgenstern, M.; Kuehl, R.; Senneville, E.; Moriarty, T. F.; Obremskey, W. T.; Zimmerli, W.; Trampuz, A.; Lagrou, K.; Metsemakers, W. J. Pathogenesis and Management of Fracture-Related Infection. *Clin. Microbiol. Infect.* **2020**, *26*, 572−578.
(28) Chun, Y. S.; Lee, D. H.; Won, T. G.; Kim, Y.; Shetty, A. A.; Kim, S. J. Current Modalities for Fracture Healing Enhancement. *Tissue Eng. Regener. Med.* **2022**, *19*, 11−17.
(29) Goodnough, L. H.; Ambrosi, T. H.; Steininger, H.; DeBaun, M. R.; Abrams, G. D.; McAdams, T. R.; Gardner, M. J.; Chan, C. K. F.; Bishop, J. A. Delayed Union of a Diaphyseal Forearm Fracture Associated With Impaired Osteogenic Differentiation of Prospectively Isolated Human Skeletal Stem Cells. *JBMR Plus* **2020**, *4*, No. e10398.
(30) Song, H.; Li, X.; Zhao, Z.; Qian, J.; Wang, Y.; Cui, J.; Weng, W.; Cao, L.; Chen, X.; Hu, Y.; Su, J. Reversal of Osteoporotic Activity by Endothelial Cell-Secreted Bone Targeting and Biocompatible Exosomes. *Nano Lett.* **2019**, *19*, 3040−3048.
(31) Li, D.; Liu, J.; Guo, B.; Liang, C.; Dang, L.; Lu, C.; He, X.; Cheung, H. Y. S.; Xu, L.; Lu, C.; He, B.; Liu, B.; Shaikh, A. B.; Li, F.; Wang, L.; Yang, Z.; Au, D. W. T.; Peng, S.; Zhang, Z.; Zhang, B. T.; Pan, X.; Qian, A.; Shang, P.; Xiao, L.; Jiang, B.; Wong, C. K. C.; Xu, J.; Bian, Z.; Liang, Z.; Guo, D. A.; Zhu, H.; Tan, W.; Lu, A.; Zhang, G. Osteoclast-Derived Exosomal MiR-214-3p Inhibits Osteoblastic Bone Formation. *Nat. Commun.* **2016**, *7*, 10872.
(32) Luo, Z. W.; Li, F. X. Z.; Liu, Y. W.; Rao, S. S.; Yin, H.; Huang, J.; Chen, C. Y.; Hu, Y.; Zhang, Y.; Tan, Y. J.; Yuan, L. Q.; Chen, T. H.; Liu, H. M.; Cao, J.; Liu, Z. Z.; Wang, Z. X.; Xie, H. Aptamer-Functionalized Exosomes from Bone Marrow Stromal Cells Target Bone to Promote Bone Regeneration. *Nanoscale* **2019**, *11*, 20884−20892.
(33) Xiong, Y.; Chen, L.; Yan, C.; Zhou, W.; Yu, T.; Sun, Y.; Cao, F.; Xue, H.; Hu, Y.; Chen, D.; Mi, B.; Liu, G. M2 Macrophagy-Derived Exosomal MiRNA-5106 Induces Bone Mesenchymal Stem Cells towards Osteoblastic Fate by Targeting Salt-Inducible Kinase 2 and 3. *J. Nanobiotechnol.* **2020**, *18*, 66.
(34) Komatsu, D. E.; Duque, E.; Hadjiargyrou, M. MicroRNAs and Fracture Healing: Pre-Clinical Studies. *Bone* **2021**, *143*, 115758.
(35) Formosa, T.; Winston, F. The Role of FACT in Managing Chromatin: Disruption, Assembly, or Repair? *Nucleic Acids Res.* **2020**, *48*, 11929.
(36) Lolis, A. A.; Londhe, P.; Beggs, B. C.; Byrum, S. D.; Tackett, A. J.; Davie, J. K. Myogenin Recruits the Histone Chaperone Facilitates Chromatin Transcription (FACT) to Promote Nucleosome Disassembly at Muscle-Specific Genes. *J. Biol. Chem.* **2013**, *288*, 7676.
(37) Hossan, T.; Nagarajan, S.; Baumgart, S. J.; Xie, W.; Magallanes, R. T.; Hernandez, C.; Chiaroni, P. M.; Indenbirken, D.; Spitzner, M.; Thomas-Chollier, M.; Grade, M.; Thieffry, D.; Grundhoff, A.; Wegwitz, F.; Johnsen, S. A. Histone Chaperone SSRP1 Is Essential for Wnt Signaling Pathway Activity During Osteoblast Differentiation. *Stem Cells* **2016**, *34*, 1369−1376.
(38) Shen, Z.; Formosa, T.; Tantin, D. FACT Inhibition Blocks Induction But Not Maintenance of Pluripotency. *Stem Cells Dev.* **2018**, *27*, 1693.
(39) Karner, C. M.; Long, F. Wnt Signaling and Cellular Metabolism in Osteoblasts. *Cell. Mol. Life Sci.* **2017**, *74*, 1649.
(40) Maupin, K. A.; Droscha, C. J.; Williams, B. O. A Comprehensive Overview of Skeletal Phenotypes Associated with Alterations in Wnt/β-catenin Signaling in Humans and Mice. *Bone Res.* **2013**, *1*, 27−71.
(41) Zalavras, C. G.; Marcus, R. E.; Levin, L. S.; Patzakis, M. J. Management of Open Fractures and Subsequent Complications. *J. Bone Jt. Surg.* **2007**, *89*, 884−895.
(42) Hao, J.; Cuellar, D. O.; Herbert, B.; Kim, J. W.; Chadayammuri, V.; Casemyr, N.; Hammerberg, M. E.; Stahel, P. F.; Hak, D. J.; Mauffrey, C. Does the OTA Open Fracture Classification Predict the Need for Limb Amputation? A Retrospective Observational Cohort Study on 512 Patients. *J. Orthop. Traumatol.* **2016**, *30*, 194−198.
(43) Haq, R. U.; Jain, A. A New Classification Scheme for Open Fractures. *J. Orthop. Traumatol.* **2011**, *25*, No. e59.
(44) Foster, A. L.; Moriarty, T. F.; Trampuz, A.; Jaiprakash, A.; Burch, M. A.; Crawford, R.; Paterson, D. L.; Metsemakers, W. J.; Schuetz, M.; Richards, R. G. Fracture-Related Infection: Current Methods for Prevention and Treatment. *Expert Review of Anti-Infective Therapy*. Taylor and Francis Ltd, April 2, 2020; pp 307−321.
(45) Pajarinen, J.; Lin, T.; Gibon, E.; Kohno, Y.; Maruyama, M.; Nathan, K.; Lu, L.; Yao, Z.; Goodman, S. B. Mesenchymal Stem Cell-Macrophage Crosstalk and Bone Healing. *Biomaterials* **2019**, *196*, 80−89.
(46) Xiong, Y.; Chen, L.; Yan, C.; Zhou, W.; Yu, T.; Sun, Y.; Cao, F.; Xue, H.; Hu, Y.; Chen, D.; Mi, B.; Liu, G. M2 Macrophagy-Derived Exosomal MiRNA-5106 Induces Bone Mesenchymal Stem Cells towards Osteoblastic Fate by Targeting Salt-Inducible Kinase 2 and 3. *J. Nanobiotechnol.* **2020**, *18*, 66.
(47) Xiong, Y.; Chen, L.; Yan, C.; Zhou, W.; Endo, Y.; Liu, J.; Hu, L.; Hu, Y.; Mi, B.; Liu, G. Circulating Exosomal miR-20b-5p Inhibition Restores Wnt9b Signaling and Reverses Diabetes-Associated Impaired Wound Healing. *Small* **2020**, *16*(). DOI: DOI: 10.1002/SMLL.201904044.
(48) Cahill, S. V.; Kwon, H. K.; Back, J.; Lee, I.; Lee, S.; Alder, K. D.; Hao, Z.; Yu, K. E.; Dussik, C. M.; Kyriakides, T. R.; Lee, F. Y. Locally delivered adjuvant biofilm-penetrating antibiotics rescue impaired endochondral fracture healing caused by MRSA infection. *J. Orthop. Res.* **2021**, *39*, 402−414.
(49) Chen, L.; Xiong, Y.; Yan, C.; Zhou, W.; Endo, Y.; Xue, H.; Hu, Y.; Hu, L.; Leng, X.; Liu, J.; Lin, Z.; Mi, B.; Liu, G. LncRNA KCNQ1OT1 accelerates fracture healing via modulating miR-701-3p/FGFR3 axis. *FASEB J.* **2020**, *34*, 5208−5222.
(50) Li, G.; Zhu, Q.; Wang, B.; Luo, R.; Xiao, X.; Zhang, Y.; Ma, L.; Feng, X.; Huang, J.; Sun, X.; Wen, Z.; Pan, Y.; Yang, C. Rejuvenation of Senescent Bone Marrow Mesenchymal Stromal Cells by Pulsed Triboelectric Stimulation. *Adv. Sci.* **2021**, *8*, 2100964.